ICAM-1 TARGETED DELIVERY AND BIODISTRIBUTION OF PROTEIN NANOPARTICLES

A Dissertation
Presented to
The Academic Faculty

by

Adaya Queen

In Partial Fulfillment
of the Requirements for the Degree
Master Chemical Engineering

Georgia Institute of Technology
August 2022

ICAM-1 TARGETED DELIVERY AND BIODISTRIBUTION

OF PROTEIN NANOPARTICLES

Approved by:

Dr. Julie Champion, Advisor
School of Chemical and Biomolecular Engineering
Georgia Institute of Technology

Dr. Manu Platt
School of Biomedical Engineering
Georgia Institute of Technology

Dr. Ravi Kane
School of Chemical and Biomolecular Engineering
Georgia Institute of Technology

Date Approved: July 13, 2022

ACKNOWLEDGEMENTS

I have truly enjoyed learning and growing during my last couple of years at Georgia Tech. I could not have asked for a better advisor, Dr. Julie Champion. Julie, thank you for consistently guiding me through the arduousness of this process and providing that gentle nudge forward to keep me going. More importantly, thank you for believing in me. To my team: Dylan, Yirui, Sydney, Thomas, Jaeyoung, Anshul, Adam, Sam, Linh, Mikaela, and Wei. Thank you so much for your support, mentorship, and friendship! I am sad to have to leave you all so soon, but I look forward to celebrating and supporting all of you in your future achievements. Thank you, Dr. Richard Noel, for all your guidance during my mouse experiments. I would not have completed the final piece of my research without your help. Thomas, thank you for helping me through 74 mice, I would still be grinding through my mouse experiments if it weren't for you.

To the United States Army and Dr. Martha Grover, thank you for affording me this fantastic opportunity to learn and grow at such an amazing institution of higher learning like Georgia Tech! I would like to thank my friends outside of my Georgia Tech family who constantly gave me a shoulder to lean on or checked on me when I was M.I.A for too long. Lastly, I would like to thank my family: Mom, Dad, and Isaiah. Your love and support mean the world to me, and I would not be here without you. Mimi ni kwa sababu sisi ni!

TABLE OF CONTENTS

LIST OF TABLES

LIST OF FIGURES

LIST OF SYMBOLS AND ABBREVIATIONS

ACE	Angiotensin Converting Enzyme
ARDS	Acute Respiratory Distress Syndrome
BCA	Bicinchoninic Acid Assay
BSA	Bovine Serum Albumin
CLP	Cecal Ligation and Puncture
COVID	Coronavirus Disease
DGCR2	Digeorge Syndrome Critical Region Gene 2
DLS	Dynamic Light Scattering
DTSSP	3,3'- Dithiobis (Sulfosuccinimidyl Propionate)
DMSO	Dimethyl Sulfoxide
DSS	Dextran Sulfate Sodium Colitis
EGFP	Enhanced Green Fluorescent Protein
EPR	Enhanced Permeability and Retention
FBS	Fetal Bovine Serum
FITC	Fluorescein Isothiocyanate
GLP-1	Glucagon-Like Peptide-1
HDV-1	Hepatic-Directed Vesicles-Insulin
ICAM	Intercellular Adhesion Molecule
IgG	Immunoglobulin G
IV	Intravenous Administration
JNK	C-Jun N-Terminal Kinase
LFA-1	Lymphocyte Function-Associated Antigen
LPS	Lipopolysaccharide

MAC-1	Macrophage Integrin
MSA	Mouse Serum Albumin
MW	Molecular Weight
NP	Nanoparticle
NF-κB	Nuclear Factor-kappa B
NSAIDS	Non-Steroidal Anti-Inflammatory Drugs
PBS	Phosphate-Buffered Saline
PCAM	Platelet Endothelial Cell Adhesion Molecule
PCL	Polycaprolactone
PDI	Polydispersity Index
PEG	Polyethylene Glycol
PEI	Polyvinyl Imine
PLGA	Poly (Lactic-Co-Glycolic Acid)
PVA	Polyvinyl Alcohol
SARS-CoV-2	Severe Acute Respiratory Syndrome Coronavirus 2
SLN	Solid Lipid Nanoparticles
SDS	Sodium Dodecyl Sulfate
TNP	Tumor Necrosis Factor
VCAM	Vascular Cell Adhesion Molecule
VLP	Virus Like Particle

SUMMARY

As a novel biomaterial, protein nanoparticles have been designed for a variety of drug delivery applications. The reproducibility and tunability of protein nanoparticles are applicable to many therapeutic applications. Since March 2020, the world has been engulfed in a pandemic that has a high rate of infection. With symptoms of severe pneumonia, cardiovascular complications, organ failures that resulted in many deaths, COVID-19 primarily targets the endothelial cells lining the vasculature of many organs such as the lungs. Although there are anti-inflammatory treatments being administered, these treatments do not specifically treat inflammation at the source and typically have negative side-effects. Therefore, there is an urgent need to develop a therapeutic that can be delivered intracellularly to regulate inflammation. The ability to conjugate functional groups onto the surface of protein nanoparticles make them a promising candidate to deliver anti-inflammatory protein therapeutics to inflamed cells which could prevent tissue and organ damage; thereby, mitigating the progression of many inflammatory diseases. However, translating these nanocarriers into the clinical setting remains a challenge as unspecific cell targeting remains a concern for nanoparticles delivery. To address this limitation, we have developed protein nanoparticles with ICAM-1 antibodies to evaluate the uptake of targeted and coated nanoparticles in endothelial cells. In addition, we assessed the biodistribution of these nanoparticles in healthy mice to determine if the conjugated coating improved targeting efficiency to vascularized endothelial cells. In response to the pandemic, we engineered protein nanoparticles with ACE2 antibodies to target endothelial cells. This work highlights engineering of a functional antibody coating to target the ICAM-1 receptors on cells to enhance nanoparticle uptake and the fabrication of mouse

serum albumin nanoparticles which were used to assess the biodistribution of the nanoparticles in mice following intravenous administration.

CHAPTER 1. INTRODUCTION

1.1 Inflammation

Inflammation is a crucial factor in many diseases and is part of the body's defense mechanism and its initial response to trauma[1]– [3]. Inflammation is the result of tissue damage that initiates vascular, molecular, and cellular events that are designed to clear out debris or pathogens and initiate repair. An inflammatory response is induced when host cells are activated by antigens on pathogens, which result in the secretion of proinflammatory cytokines and chemokines expressed by myeloid cells like microphages, monocytes, and dendritic cells. Inflammation has been historically defined as comprising symptoms of swelling, redness, warmth, pain, heat, and joint immobility. There are many causes of inflammation: physical trauma, chemical trauma, infectious micro-organisms, and many diseases including autoimmune diseases. Through these causes, inflammation can be categorized as acute or chronic.

There are two defining categories of inflammation: acute and chronic. Acute inflammation typically lasts for a shorter duration, eliminating injurious agents while initiating the repair process[1]. An example of acute inflammation is that resulting from a bacterial infection. On the other hand, chronic inflammation lasts weeks to years, contributing to the progression of tissue damage due to repeated acute injury and/or impaired resolution of inflammation. Chronic inflammation is the leading cause of death worldwide, where three out of five individuals die[4]. Cancer, obesity, inflammatory bowel disease, and diabetes are some examples of many diseases that are the cause or are associated with chronic inflammation. Recently, the most impactful disease that exacerbates hyperinflammation has been attributed to the coronavirus disease 2019

(COVID-19), with more than 163 million confirmed cases and 5.9 million deaths worldwide[5], [6].

Common symptoms of COVID-19 include fatigue, shortness-of-breath, and brain fog [[5]. In severe cases, patients exhibited a dysregulated immune/inflammatory response that led to tissue damage, organ failure and, in some cases, death within 6-12 months after initial onset of COVID-19[5]. Therapies targeting inflammation have been researched to understand the inflammatory pathways to enable further therapeutic advancements. Currently, there is no curative drug that specifically treats COVID-19. Researchers have explored therapeutic options such as convalescent plasma therapy, the transfusion of blood from a recovered COVID-19 patient to a patient with the infection, non-steroidal anti-inflammatory drugs (NSAIDS), T-cell targeted therapies, cytokine inhibitors, and corticosteroids have been evaluated to suppress the inflammation [6]. However, these options had varying results, with some adverse effects, and were unsuccessful in significantly reducing inflammation or mortality rates. Ultimately, there is a need for new anti-inflammatory therapeutics that are safe and effective.

Microbes, both pathogens and commensals, have evolved highly effective mechanisms to modulate the immune system through active manipulation of regulators of the inflammatory response. AvrA is a Salmonella enzyme that functions in the cytosol to acetylate key serine and threonine residues on MKK4/7, which inhibits phosphorylation of the JNK pathway and prevents cell apoptosis[7], [8]. In addition, AvrA indirectly deubiquitinates IκBα by an unknown mechanism that stabilizes phosphorylated-IκBα and prevents additional phosphorylation, blocking the transcription of nuclear factor-κB (NF-κB)[8]. AvrA is a promising anti-inflammatory, anti-apoptotic protein that can potentially work against several chronic diseases. A challenge of AvrA as a new therapeutic is the delivery of the protein to the cytosol of the cell. Therefore, we propose preclinical validation of AvrA to treat hyper-inflammation via development of protein nanoparticles that will deliver AvrA to the cytosol of SARS-CoV-2 infected or susceptible cells to arrest inflammation at the source.

1.2 Nanoparticles for Protein Delivery

Nanoparticles have been developed as drug carriers for treatment of various diseases that require the delivery of therapeutic agents to a target tissue or cell type. Conventional therapeutic methods such as small drugs and chemotherapy have limitations such as poor biodistribution, low efficiency, non-specific targeting, and undesirable side effects[9], [10]. In cancer treatment for example, nanoparticle drug delivery systems have been shown to overcome drug resistance, be precise in the targeting of tumor cells, demonstrate reduction of side effects, and promote good pharmacokinetics [11]. Using recombinant protein engineering, many therapeutic proteins have been developed to treat a plethora of diseases including autoimmune and inflammatory diseases, genetic disorders, cancers, and infectious diseases[12]. Despite the advantages of nanoparticles in delivering small hydrophobic drugs, these therapeutic drug delivery systems must overcome the additional challenges that accompany protein therapeutics, including instability, immunogenicity, and limited permeability through biological barriers due to large size and hydrophilic surface. Different kinds of nanoparticles have been used for protein delivery. Some existing nanoparticles have been adapted for protein while others have been newly created for protein cargo.

1.2.1 Lipid Nanoparticles

Liposomes and solid lipid nanoparticles (SLNs) are two common lipid-based nanoparticles. Liposomes are spherical vesicles with an aqueous core that consist of a phospholipid layer with hydrophilic compounds enclosed in the core and hydrophobic compounds in the lipid membrane. SLNs have solid cores at room temperature and provide some additional protection against degradation. Liposomes are the first functionalized nanoparticle drug delivery system that has been successfully administered through different routes such as parenteral, oral, pulmonary, nasal, ocular, and topical[12]. One example of therapeutic liposome treatment is the use of hepatic-directed vesicles-insulin (HDV-1), an insulin containing diabetic treatment that is delivered orally and subcutaneously to target the hepatocytes of the liver. These liposomes have been tested in phase II clinical trials and contain a hepatocyte targeting molecule that showed to be an effective insulin replacement treatment with very low toxicity and successful targeting in insulin deficient animals[13]. Proteins such as Dendra2, eGFP, and other peptides have been successfully incorporated into mammalian cells using fusogenic liposomes where the carrier membrane is fused with cell membrane and the protein cargo is released into the cytosol[14]. Solid lipid nanoparticles have been successfully loaded with enrofloxacin, an antibiotic, used to enhance intracellular delivery and efficacy against *Salmonella*[15]. SLNs are a promising drug carrier system alternative due to their biocompatibility, stability, and cost effectiveness; however, they have low drug loading efficiency and drug expulsion and burst release due to crystallization process[15], [16]. The advantage of liposomes as a therapeutic delivery system is that they are biocompatible, non-immunogenic, provide sustained drug release, and have minimal side effects. Some of the disadvantages of liposomes include encapsulation limitations, irregular particle size distributions, and the use of organic solvents that can impact protein stability and safety in clinical applications[12], [17].

1.2.2 Polymer Nanoparticles

Polymeric nanoparticles have been studied extensively in the pharmaceutical field because their surface and size are easily tuneable. Like lipid nanoparticles, polymer nanoparticles have difficulty encapsulating proteins as various organic solvents are essential for fabrication, which can denature the proteins or negatively impact their biological functionality[18]. Some synthetic polymer materials that are biocompatible and biodegradable, non-toxic, and stable are poly (lactic-co-glycolic acid) (PLGA), polyvinyl imine (PEI), polycaprolactone (PCL), and polyvinyl alcohol (PVA)[17], [19], [20]. The functionality of drug release in polymer nanoparticles is dependent upon the particle size, chain length, protein loading amount, and environmental changes such as pH and temperature[21]. One example of intracellular delivery of protein using polymeric nanoparticles, is the use of polybutylcyanoacrylate (PBCA) with apolipoprotein E coatings to improve uptake across the blood-brain barrier (BBB) and delivery into neurons[22]. PLGA nanoparticles have been developed to release loaded bone morphogenetic protein (BMP-2) for bone regeneration using mesenchymal stromal cells. In certain applications, protein encapsulation using polymer nanocarriers are hindered by uncontrolled release and protein denaturation[23]. Additionally, aggregation and toxicity are potential disadvantages to polymer nanoparticles[24], [25].

1.2.3 Inorganic Nanoparticles

Inorganic nanoparticles are often very porous which gives the advantage of a larger surface area to volume ratio and an easily modified surface conjugation chemistry than organic nanoparticles[26]. Gold nanoparticles, silica nanoparticles, magnetic nanoparticles, quantum dots, and carbon nanotubes are the common inorganic nanoparticles that have been studied[25]. Silica nanoparticles are known to be non-immunogenic, inert, and easily modifiable as therapeutic agents. Gold nanoparticles have been extensively used due to its biocompatibility, spectroscopic properties, and ease of modifying the surface via thiol group[21], [26]. Ghosh et al. used functionalized gold nanoparticles, coated with a short peptide, to intracellularly deliver a membrane-impermeable enzyme in active form to a variety of cell lines[27]. Lee et al. demonstrated that gold nanoparticles conjugated to DNA and complexed with cationic endosomal disruptive polymers can deliver Cas9 ribonucleoprotein into a wide variety of cell types; efficiently correcting DNA mutations that cause Duchenne muscular dystrophy with minimal off-target DNA damage when assessed in mice[28]. These inorganic nanoparticles improve the transport and loading efficiency of therapeutic drugs and are easily modified via the integration of various functional groups. However, the biosafety of inorganic nanomaterials and slow biodegradation rates may be a challenge in clinical applications[17].

1.2.4 Hybrid Nanoparticles

Hybrid nanoparticles are comprised at least two different materials and present new properties and functionalities that are not possible for single-component nanoparticles. As a hybrid drug delivery system, the properties of the nanoparticle allow for enhanced treatment efficacy and reduced drug resistance[21], [26]. A newly designed hybrid nanoparticle comprised of a fluorescent inorganic silica core with a biocompatible polymer shell and a terminal unit to facile conjugations via click chemistry has demonstrated the potential to be biocompatible carriers for intracellular delivery via in vitro experiments on lung cancer cells[29].

1.2.5 Protein Nanoparticles

Protein nanoparticles are a unique alternative to all other classes of nanoparticles because they are comprised entirely of protein. Therefore, the therapeutic protein drug can either be incorporated as the cargo or be a direct building block of the nanoparticle itself. Not only are protein nanoparticles biodegradable but they are usually fabricated using milder processes than synthetic nanoparticles. Self-assembly and desolvation are two strategies implemented to fabricate protein nanoparticles. Self-assembled nanoparticles are formed via noncovalent interactions such as hydrophobic or electrostatic forces[30]. One example of self-assembled nanoparticles is virus like particles (VLP). These particles mimic the structure of viruses, yet do not contain the viral enzyme protease, reverse transcriptase, and integrase [31], [32]. Voelkel et al. reported that they were able to deliver green fluorescent protein (GFP) and functional Flp recombinase to cells using murine retroviral particles[33]. However, the encapsulation efficiency of VLPs is limited by the number of protein subunits that make up the capsid[34]. Desolvation is a fabrication technique that allows for varied particle size depending on the protein concentration, solvent, desolvant, volume, pH, temperature, and crosslinker [16]. Using this method, an organic desolvent, such as acetone or ethanol, is continuously added to a protein dissolved in a solvent, which force the proteins to cluster together [36]. Then, a crosslinker is added to stabilize the clusters of protein into nanoparticles. Optimizing this fabrication technique to obtain the proper nanoparticle size and polydispersity can be challenging. However, the advantage of this method is that it is reproducible and stable over periods of time and can be implemented with a variety of proteins [36].

Our lab has adapted a protein desolvation process that incorporates AvrA, an effector protein from Salmonella, into a condition responsive cross-linked protein nanoparticle that can un-crosslink in the reducing environment inside cells, while maintaining the bioactivity of AvrA. Moreover, previous work has demonstrated that AvrA delivered by protein nanoparticles can suppress proinflammatory pathways *in vitro* and tissue inflammation *in vivo*. Our lab has conducted two murine dextran sulfate sodium colitis (DSS) models following transrectal delivery of AvrA and enhanced green fluorescent protein (eGFP) particles targeting the colon and observed a reduction in clinical symptoms and histological indices[7], [37]. In previous work, the delivery routes have been localized; however, to treat inflammation that is more systemic, intravenous delivery and targeting is needed.

1.3 Targeting with Protein Nanoparticles

The development of targeted drug delivery systems allows for effective transport of functional molecules and their release into diseased tissues. There are both passive and active forms of targeting. Passive targeted delivery refers to the circulation of nanoparticles in the bloodstream that can localize in tissues primarily by passive diffusion via enhanced permeability and retention (EPR) [[38], [39]. When EPR is not suitable or inefficient to selectively deliver nanoparticles to diseased tissues, nanoparticles are conjugated with targeting ligands such as small molecules, antibodies, peptides, engineered proteins, or nucleic acids which enable direct targeting of these particles to certain cell types.

Vascular endothelium is a prime target for drug delivery. The endothelium is involved in the pathological processes of inflammation and represents an important drug delivery target[40]. Intercellular adhesion molecules (ICAMs) are glycoproteins that are present on the surface of many cells and are ligands for lymphocyte function-associated antigen (LFA-1) and macrophage integrin (MAC-1). ICAM-1 is functionally involved in inflammation and expression is enhanced constitutively with inflammation[40]. ICAMs play a crucial role in immune and inflammatory responses; particularly, in signal transduction pathways through outside-in signaling events. However, ICAM-1 is not readily internalized by endothelial cells by itself. When incorporated into nanoparticles, these anti-ICAM particles are internalized in a unique actin dependent process requiring the activation of protein kinase C[40]. This ICAM mediated endocytosis is distinct from caveolar and clathrin mediated endocytosis. Another glycoprotein that is expressed on endothelial cells is platelet endothelial cell adhesion molecule 1 (PECAM-1). PECAM-1 is highly expressed by endothelium; however, some literature reports that PCAM-1 expression is not increased by inflammation[41], [42]. Previous research has proven that ICAM-1 targeted nanoparticles exhibit superior targeting to inflamed vasculature following intra-arterial and intravenous administration[40], [41], [43]. Therefore, anti-ICAM nanoparticles appear to be well-suited for targeted delivery of therapeutic enzymes to endothelial cells and may provide a basis for treatment of hyperinflammatory diseases like COVID-19.

1.4 Motivation and Objectives

Inefficient targeting and other biological barriers severely limit the delivery of nanoparticles in biological environments. The goal of this research is to understand how desolvated protein nanoparticle uptake and biodistribution be modulated by addition of targeting antibodies. This knowledge allows us to engineer nanoparticles that enhance intracellular delivery of therapeutic proteins and minimize nonspecific delivery.

There is a myriad of hyperinflammatory diseases such as SARS-CoV-2, rheumatoid arthritis, diabetes, and inflammatory bowel syndrome that would benefit from targeted protein delivery of therapeutic drugs. A drug is only as good as its delivery system - meaning if the drug is unable to get to the inflamed cells or immune actuators, its pharmacological capabilities are irrelevant. The main objectives of this thesis are: (1) to assess desolvated protein nanoparticle uptake in different cell lines using various antibody coatings, (2) to fabricate and optimize targeted protein nanoparticles for in vivo use, and (3) to enhance protein nanoparticles delivery to achieve targeted, intracellular delivery of coated nanoparticles.

1.5 Thesis Overview

The overall goal of this thesis is to investigate the delivery of targeted coated nanoparticles and assess the biodistribution in healthy mice. To accomplish the objectives, outline in the previous section, Chapter 2 details the engineering of a functional antibody coating to target the ICAM-1 receptors on cells to enhance nanoparticle uptake and Chapter 3 focuses on the fabrication of mouse serum albumin nanoparticles and the biodistribution of the targeted nanoparticles in mice following intravenous administration.

CHAPTER 2. ENGINEERING ICAM-1 TARGETING PROTEIN COATINGS TO ENHANCE NANOPARTICLE DELIVERY IN VITRO

2.1 Introduction

Nanoparticles have been heavily investigated in drug delivery and medical applications[18], [20], [44]–[47]. In the previous chapter, we discussed the impact of chronic inflammation and the emerging class of protein based intracellular therapeutics that can target specific intracellular pathways. A major obstacle in the treatment of various diseases is the delivery of therapeutic agents to the target area. Nanoparticles have been proven to overcome delivery challenges. In our lab, we have fabricated bovine serum albumin particles (BSA), but BSA alone does not have specific targeting properties. Albumin binding proteins have been identified on a variety of cell lines and tissues. Due to the abundance of receptors on multiple cell types, BSA lacks the ability to target specialized receptors on specific cell types[48], [49]. Thus, BSA NPs could non-specifically interact with undesired cells and would not have a high affinity to targeted cells involved in inflammation. This obstacle could be overcome by decorating the surface of nanoparticles with high affinity specific targeting ligands to enhance selective delivery of therapeutic drugs to desired cell types.

Antibodies, proteins, small molecules, and peptides are typically used as targeting ligands for targeting inflammation in cancer tumors and endothelial cells. Selectins and cellular adhesion molecules (CAMs) are the main kinds of inflammation-involved molecules. P-selectin, L-selectin, E-selectin, ICAM-1, and VCAM-1 are highly expressed receptors that are used to target inflamed vascular endothelium[50]. P-selectin glycoprotein ligand 1 (PSGL 1) was presented on the surface of liposomes to actively target tumor cells using a novel streptavidin molecule to successfully target selectins [51]. In addition, anti-VCAM-1 has been adsorbed onto iron oxide nanoparticles and shown increase specificity and affinity to recombinant human VCAM-1 chimeras [46]. Expression of CAMs are locally induced or enhanced at areas of inflammation and are an easily accessible targeting molecule for therapeutics circulating in the blood[52], [53]. Although ICAM-1 is present on several cell types, the level of ICAM-1 expression is orders of magnitude higher on vascular endothelial cells[54]–[57]. Compared to selectins, once ICAM-1 is upregulated, it remains on the cell surface for more than 48 hours[58]. Ultimately, ICAM-1 is well suited as the targeting receptor for the following reasons: (1) ICAM-1 is highly expressed on the surface of endothelial cells and is (2) functionally involved in inflammation while selectively (3) internalizing 100-300nm diameter conjugates, but not monomolecular antibodies or conjugates, and (4) allows for the delivery and release of cargo across cells to the site of inflammation [54]–[57], [59]. A targeting ligand incorporated onto BSA NPs could improve specific targeting and affinity to receptors, which may improve the efficacy of these nanoparticles as a delivery system to target cells involved in inflammation.

Severe acute respiratory syndrome coronavirus 2 (SARS-CoV-2) is a virus that primarily targets the lungs, systemic small vessels, and immune organs resulting in decreased immune function and pneumonia and may progress into acute respiratory distress syndrome (ARDS) [[60]. Like all viruses, SARS-CoV-2 has proteins on the viral capsid that have evolved to specifically target cell surface receptors of host cells to increase viral uptake and replication. SARS-CoV-2 infects host cells by binding the surface receptor of angiotensin converting enzyme 2 (ACE-2) via the surface spike protein, where it releases RNA and is cleaved by a serine protease TMPRSS2, facilitating the fusion between the viral and host membranes [7]– [9]. ACE-2 protein is expressed in lung and small intestine epithelial cells, arterial and venous endothelial cells, and vascular smooth muscle cells[62]. The abundance of ACE2 receptors in the epithelial and endothelial cells provide multiple routes of systemic SARS-CoV-2 infection in the body.

In severe cases, SARS-CoV-2 is associated with pneumonia, acute respiratory syndrome, and kidney failure[63]. These symptoms are accompanied by hyperinflammation, neutrophilia, and hypoxia[64]. Usually, the first line of immune defense is a coordinated, regulatory response to mitigate infection or repair injured tissue[64], [65]. However, excessive inflammatory responses results in destructive tissue and organ damage. There have been attempts to use ACE2 inhibitors and blockers by targeting the host cells; however, these methods have been shown to increase the risk of COVID-19 infection by upregulating ACE2[65]. Monoclonal antibodies such as Tocilizumab and Sarilumab have been utilized to reduce the detrimental effects of SARS-CoV-2. The cytokine, Interleukin-6 (IL-6), is one of the key cytokines responsible for the inflammatory effects of SARS-CoV-2. Tocilizumab and Sarilumab are IL-6 receptor antagonists that have been used to manage severe cases of COVID-19, rheumatoid arthritis, and cytokine release syndrome[65], [66].

Other small molecule drug treatments have been tested and evaluated for their effectiveness in targeting SARS-CoV-2. Remdesivir, also known as Veklury, is an antiviral drug that inhibits viral replication by terminating RNA transcription[65]–[67]. Remdesivir has been shown to shorten the time to recovery in COVID-19 patients and minimize respiratory tract infections. Some of the adverse effects of this drug include respiratory failure, anemia, hypersensitivity, and hyperglycemia[67]. Dexamethasone, a corticosteroid, has also been used to inhibit lung inflammation in SARS-CoV-2 infected patients[67], [68]. However, these drugs have low specificity towards inflamed cells and produce adverse side effects when administered. An effective therapy to treat hyperinflammation would target host cells susceptible to SARS-CoV-2 infection and regulate the inflammatory response. In this chapter, we propose to covalently coat therapeutic protein nanoparticles with the ICAM-1 antibody to effectively target endothelial cells, especially inflamed cells, and the ACE-2 antibody to target cells susceptible to the SARS-CoV-2 virus. The success of this work would create a new drug delivery protein nanoparticle that could potentially be used to successfully deliver an anti-inflammatory protein drug, like AvrA, to suppress systemic inflammation.

2.2 Methods

2.2.1 BSA Nanoparticle Fabrication

Bovine Serum Albumin (BSA) nanoparticles were fabricated using a desolvation method[69]. 10 mg of BSA was dissolved in 1 mL Milli-Q water (18.2 MΩ·cm). Then, 400 µL of acetone desolvent was added dropwise at 1 mL/min to 100 µL of protein solution. Next, 3,3'-dithiobis (sulfosuccinimidyl propionate) (DTSSP) was added in a molecular ratio of 2.2 molecules lysines present in the protein to one molecule DTSSP and the solution was mixed on a stir plate at 700 rpm. After mixing for one hour, the protein nanoparticles were centrifuged at 10,000 x g for 10 minutes. The supernatant was removed, and the pellet was resuspended in 0.5 mL of phosphate buffered saline (PBS, pH 7.4). The nanoparticles were sonicated twice on ice for 1 minute, with 2 second pulses at 60% amplitude. The nanoparticles were then centrifuged for 5 minutes at 700 x g at 4 ˚C and the supernatant was collected while the pellet was discarded. This centrifugation step was repeated twice.

2.2.2 Alexa Fluor-488 Fluorescent Nanoparticle

AlexaFluor 488 5-SDP Ester (Thermo Fisher Scientific) was dissolved in dimethyl sulfoxide (DMSO) according to the manufacturer manual. 10 mg BSA and Alexa Fluor 488 dye were mixed at a ratio of 0.4 mg of protein to 1 µL of dye in 1M sodium bicarbonate solution (pH=8.3) and stirred continuously at room temperature for 1 hour. After conjugation, excess dye was removed through filtered centrifugation cycles using a 10 kDa molecular weight cutoff filter buffer exchanged to phosphate-buffered saline (PBS, pH 7.4). Degree of labeling and the final protein concentration was measured using the fluorescent dye labeling settings on a NanoDrop 2000. To make fluorescent NPs, the nanoparticle fabrication and characterization procedures described above were used to fabricate fluorescent protein nanoparticles.

2.2.3 Covalent Protein Coatings

Anti-ACE2 Coatings: The ACE-2 targeting antibody used was monoclonal (CL4013) mouse IgG recognizing mouse, human, and rat ACE-2 (Thermo Fisher Scientific). 500 µg of BSA NPs, 5 µg/mL anti-ACE2 antibody (the volume of the solution was adjusted to 200 µL with PBS), and 0.1 mg of DTSSP were mixed in a 1.5 mL eppendorf tube. Samples were reacted for 12 hours at 4°C under constant stirring of 1200 rpm. Once the reaction was complete, 25 µL of 1 M Tris base (pH = 7.6) was added to the nanoparticles to quench unreacted DTSSP for 10 minutes on a stir plate. Nanoparticles were then collected using centrifugation (15,000 x g, 10 mins, 4°C) and the pellets were resuspended in 200 µL of sterile PBS. The nanoparticles were sonicated twice on ice for 1 minute, with 2 second pulses at 60% amplitude. Nanoparticle concentration was assessed using BCA assay and the size distribution was measured using DLS. When appropriate, the amount of anti-ACE2 was changed to 10 µg/mL, 50 µg/mL, and 100 µg/mL.

Anti-ICAM1 Coatings: The ICAM-1 targeting antibody used was monoclonal (CD54/R6.5) mouse IgG recognizing human ICAM-1(Thermo Fisher Scientific). 500 µg of BSA NPs, 5 µg/mL anti-ICAM1 antibody (the volume of the solution was adjusted to 200 µL with

PBS), and 0.1 mg of DTSSP were mixed in a 1.5 mL eppendorf tube. Samples were reacted for 12 hours at 4°C under constant stirring of 1200 rpm. Once the reaction was complete, 25 µL of 1 M Tris base (pH = 7.6) was added to the nanoparticles to quench unreacted DTSSP for 10 minutes on a stir plate. Nanoparticles were then collected using centrifugation (15,000 x g, 10 mins, 4°C) and the pellets were resuspended in 200 µL of sterile PBS. The nanoparticles were sonicated twice on ice for 1 minute, with 2 second pulses at 60% amplitude. Nanoparticle concentration was assessed using BCA assay and the size distribution was measured using DLS. When appropriate, the amount of anti-ICAM1 was changed to 10 µg/mL, 50 µg/mL, and 100 µg/mL.

IgG Coatings: 500 µg of BSA NPs, 5 µg/mL anti-human IgG (the volume of the solution was adjusted to 200 µL with PBS), and 0.1 mg of DTSSP were mixed in a 1.5 mL eppendorf tube. Samples were reacted for 12 hours at 4°C under constant stirring of 1200 rpm. Once the reaction was complete, 25 µL of 1 M Tris base (pH = 7.6) was added to the nanoparticles to quench unreacted DTSSP for 10 minutes on a stir plate. Nanoparticles were then collected using centrifugation (15,000 x g, 10 mins, 4°C) and the pellets were resuspended in 200 µL of sterile PBS. The nanoparticles were sonicated twice on ice for 1 minute, with 2 second pulses at 60% amplitude. Nanoparticle concentration was assessed using BCA assay and the size distribution was measured using DLS. When appropriate, the amount of IgG was changed to 10 µg/mL, 50 µg/mL, and 100 µg/mL.

2.2.4 Nanoparticle Characterization

Protein nanoparticle size distribution were determined using Dynamic Light Scattering (DLS) with a Malvern Zetasizer Nano ZS90. Each sample was measured 3 times and each measurement had 10 runs with a dispersion medium of PBS. Protein nanoparticle concentrations were assessed using a BCA Assay according to the manufacturer's instructions (Thermo Scientific, Waltham, MA).

2.2.5 SDS-PAGE

Nanoparticle composition was determined using gel electrophoresis by heating 50 ug of NPs in sodium dodecyl sulfate polyacrylamide gel electrophoresis (SDS-PAGE) loading buffer (VWR) for 5 minutes at 95°C and loaded into a 12% SDS polyacrylamide gel at 180 V for 75 min. SDS-Gel was then stained using Coomassie blue and washed with water overnight.

2.2.6 Identifying Antibody Coating

BSA nanoparticles were fabricated and conjugated with anti-ACE2 and anti-ICAM1. Bare BSA, anti-ACE2- BSA, and anti-ICAM1-BSA nanoparticles were incubated with 2% (w/v) BSA in PBS at room temperature for 30-60 minutes. There were rinsed with PBS and collected using centrifugation (15,000 x g, 10 mins, 4°C). The pellets were resuspended in 300 µL of 2% (w/v) BSA and 1ul of antibody (mouse-IgG) and incubated for 60 minutes at room temperature. The nanoparticles were rinsed with PBS and collected using centrifugation, twice. The nanoparticles were analyzed using flow cytometry.

2.2.7 A549 Cells

A549 cells, human alveolar basal epithelial cells, (ATCC CCL-185) were cultured in complete media containing 1% penicillin and streptomycin, 10% fetal bovine serum (FBS) and Ham's F-12K Medium (Kaighn's Modification of Ham's F-12 Medium). Cells were cultured in a 75 cm^2 flask with 18 ml media/flask until ~ 80% confluent. Passages 5-12 were used in this work.

2.2.8 HUVEC Cells

Human umbilical vein endothelial (HUVEC) cells (ATCC CRL-1730) were cultured in complete media containing 1% penicillin and streptomycin, 10% fetal bovine serum (FBS), 0.1 mg/ml heparin, 50 ug/mL of endothelial cell growth media from bovine neural tissue, and Ham's F-12K Medium (Kaighn's Modification of Ham's F-12 Medium). Cells were cultured in a 75 cm^2 flask with 18 ml media/flask until ~ 90% confluent. Passages 2-10 were used in this work.

2.2.9 Flow Cytometry

Nanoparticle uptake was assessed using flow cytometry. Fluorescent nanoparticles were fabricated as previously described with BSA containing 10 wt% AlexaFluor 488-conjugated BSA. 3 x 10^4 HUVEC or A549 cells were plated in triplicate in a 48-well dish overnight. 30 μg of corresponding protein nanoparticle treatments were incubated with cells for 12 hours at 37°C. Cells were washed once with ice cold PBS, briefly trypsinized, filtered with a cell strainer (VWR) and resuspended in chilled trypan blue to quench external fluorescence. Then, cells were analyzed using a Beckman Coulter CytoFLEX. Gating was established using cells without exposure to nanoparticles, and all conditions were run with triplicates. Positive uptake events were identified as cells with an increase in fluorescein isothiocyanate (FITC) fluorescence compared to a PBS treated control.

2.2.10 Confocal Microscopy

A549 or HUVEC cells were seeded at a density of $2x10^4$ cells per well in a 6-well chamber with No. 1.5 coverslip glass bottoms (Mattek) in growth medium. After 24 hours, cells were incubated with fresh PBS with 20 ug of BSA particles with and without coatings (ICAM-1, ACE-2, and IgG) for 4 hours. Cells were washed three times with ice cold PBS and fixed with 3.7%

paraformaldehyde for 15 minutes at room temperature. Cells were permeabilized with 1% Triton X-100 in PBS for 15 minutes at room temperature and rinsed three times in PBS. Cells were incubated with 0.0528 μM rhodamine phalloidin (Biotium) in blocking buffer for 15 minutes at room temperature to stain for actin, and cell nuclei were stained with 0.02 μM Hoechst 33342 for 20 minutes at room temperature. Cells were washed three times after each stain with PBS and imaged with a PerkinElmer Spinning Disk Confocal.

2.3 Results and Discussion

2.3.1 Protein Nanoparticle Fabrication and Characterization

Antibodies were crosslinked on BSA protein nanoparticles with DTSSP for 12 hours at 4°C under constant stirring at 1200 rpm. After quenching with Tris-Base, the nanoparticles were collected using centrifugation and visualized by SDS-PAGE (Figure 2.1A). SDS-PAGE was used to visualize the mass and molecular weight composition of the various antibody coatings (anti-ICAM-1 and anti-ACE2) on each nanoparticle. Using this technique, we established that some of the protein nanoparticles did break apart during gel migration and are retained at the top of the gel in the bottom of the loading wells. This result was expected when engineering protein nanoparticles held together by a reducible crosslinker, like 3,3'-dithiobis (sulfosuccinimidyl propionate), whose central disulfide bond can be cleaved with reducing agents.

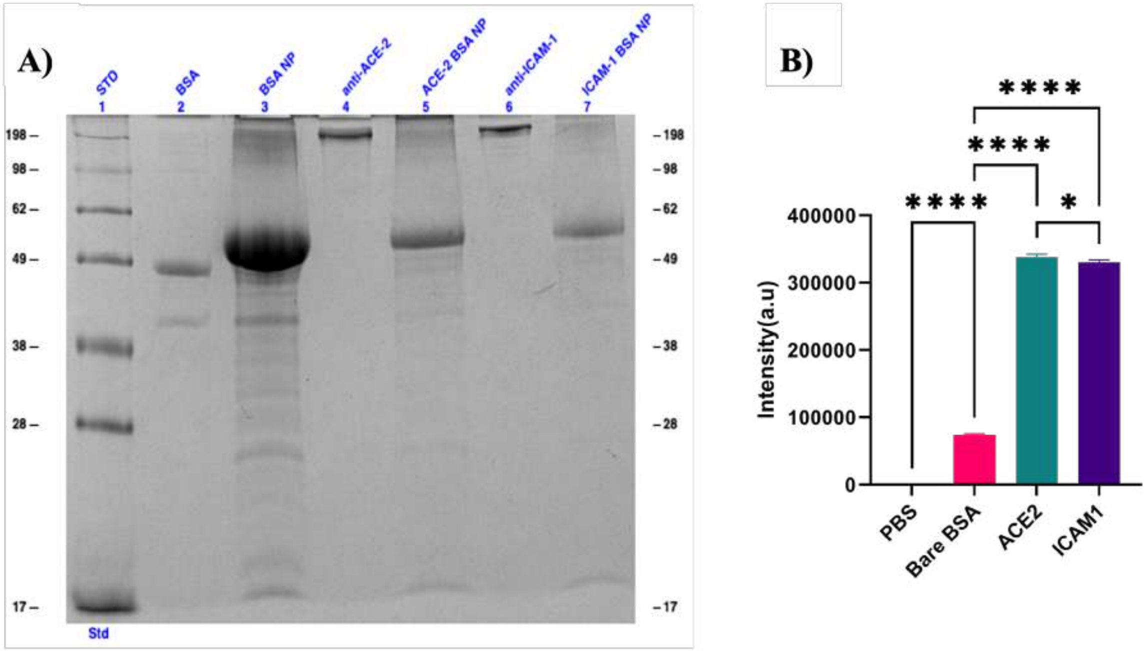

Figure 2.1 Characterization of BSA NPs. A) SDS-PAGE of bare BSA, ACE-2, and ICAM-1 NPs. B) Flow cytometry data using secondary antibody to bind the Fc region of the ACE-2 and ICAM-1 NPs to determine coating.

To prove that the antibody coatings were present on the BSA NPs, the NPs were blocked with 1% BSA solution and incubated for an hour with fluorescent anti-Mouse IgG to target the Fc receptors of the mouse ICAM1 and ACE2 antibodies and confirmed via flow cytometry (Figure 2.1B). The low fluorescent signal of the Bare NPs may be due to non-specific binding of IgG that adsorbed to the NP surface despite washing and blocking. However, the anti-ICAM1 and anti-ACE2 coated NPs show much higher labeling with fluorescent anti-mouse IgG. Therefore, it can be concluded that the antibody coatings are present.

Nanoparticle size is one of the most important physiochemical properties that influence the interaction between the nanoparticle and the cell. In addition, size plays an important role in how the body responds to, distributes, and clears nanoparticles. When particles are smaller than 20nm in diameter, the nanoparticles pass through tight endothelial junctions and are quickly cleared from circulation. Larger particles, greater than 1µm, are rapidly phagocytosed[70], [71]. Nanoparticles must be larger than 20nm to avoid filtration by the kidney, and smaller than 100 nm to avoid accumulation in the spleen and liver. However, it has been demonstrated that particles larger than 200nm will be cleared by Kupffer cells of the liver[71]. Therefore, it is imperative that the fabricated protein nanoparticles are between 100-200nm in size. Using Dynamic Light Scattering (DLS), fabrication bare BSA and coated BSA nanoparticles were confirmed to be 200nm in size (Figure 2.2 and 2.3).

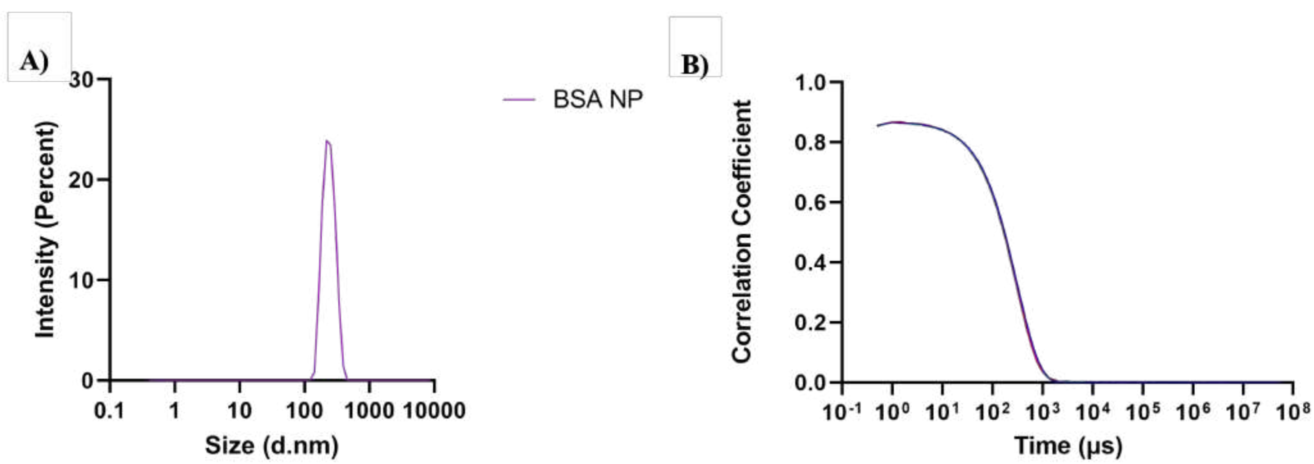

Figure 2.2 Characterization of BSA NPs. A) Size distribution overlay of BSA NPs using dynamic light scattering (DLS). B) DLS correlogram overlay of BSA NPs confirming the similar size of all nanoparticles. Exponential decay occurs around a 200 µs lag time correlating to a 200 nm hydrodynamic diameter for the nanoparticles.

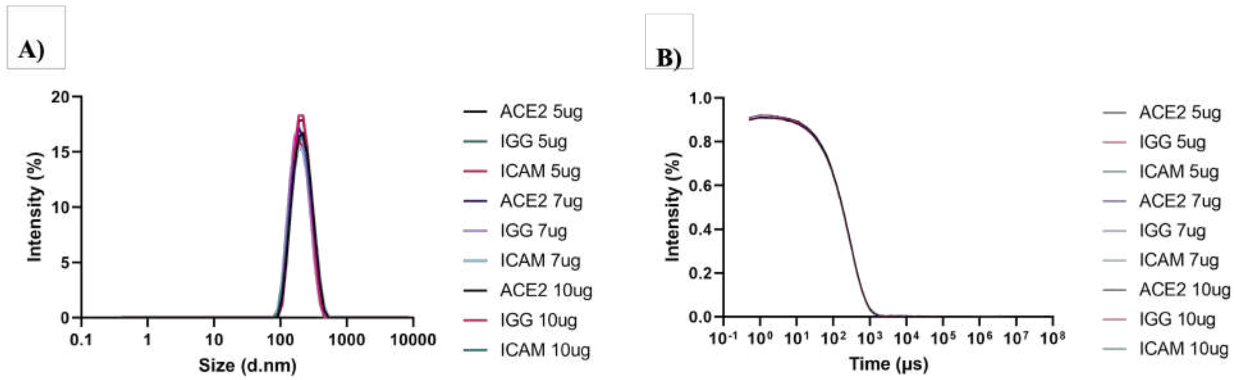

Figure 2.3 Characterization of BSA NPs. A) Size distribution overlay of BSA NPs with conjugated ACE-2, ICAM-1, or IgG antibodies at 5,7, and 10 ug/ml using dynamic light scattering (DLS). B) DLS correlogram overlay of BSA NPs confirming the similar size of all nanoparticles. Exponential decay occurs around a 200 µs lag time correlating to a 200 nm hydrodynamic diameter for all three nanoparticles (anti-ACE2, anti-ICAM1, IgG). The overlapping length of exponential decay indicates similar size distributions for all NPs.

2.3.2 Cellular Responses

2.3.2.1 Specific and Functional Coating Verification

The specificity of the various crosslinked coatings was assessed by incubating them with A549 cells. The hypothesis was that in A549 cells, a human alveolar basal epithelial cell line, anti-ACE2 coated NPs would have reduced or similar uptake to bare BSA NPs because there are few ACE2 receptors to target[72]. In this flow cytometry experiment, nanoparticle uptake was evaluated with bare, crosslinked anti-ICAM-1 coating, anti-ACE2 coating, and IgG coating. All crosslinked coatings had a concentration of 5 ug/ml (Figure 2.4). Between the bare BSA NPs and the anti-ACE2 coated NPs, the internalization of nanoparticles was similar which satisfied the hypothesis given the low expression levels of ACE2 receptors in A549 cells. Non-specific IgG showed more uptake than BSA and anti-ACE-2 which highlight the FcR interactions of the antibody with the cells [73]. The anti-ACE2 and anti-ICAM1 coatings could also bind to the neonatal Fc receptors on the A549 cell surface, indicating that Fc- receptor endocytosis could be an alternative pathway for nanoparticle internalization.

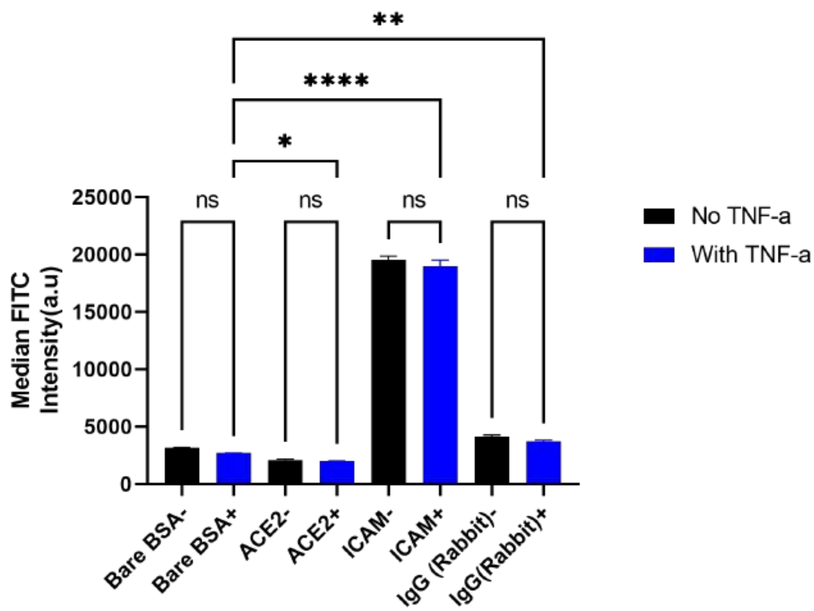

Figure 2.4 Protein nanoparticle uptake in A549 cells. (n=3, One-way ANOVA, *p<0.05, **p<0.01, ****p<0.0001)

ICAM-1 coated BSA NPs had four times more uptake than all the other nanoparticles in the A549 epithelial cells. A549 cells express ICAM-1 receptors which corroborates the uptake without TNF- a stimulation. There is a lack of research on the effect of proinflammatory cytokine TNF-a on A549 cells; however, based on the literature on the upregulation of ICAM-1 receptors in many cell types including smooth muscle cells, keratinocytes, intestinal epithelial cells, and endothelial cells it was expected that TNF-a stimulation would induce more uptake of ICAM coated nanoparticles[74]–[76]. Previous studies have shown that the upregulation of ICAM-1 is dose dependent and time dependent [76]. In Figure 2.4, A549 cells were treated with 10 ng/ml of TNF-a for 12hrs and then flow cytometry was conducted. If this experiment was repeated, treating cells with 20 ng/ml of TNF- a for 24 hours and measuring ICAM-1 expression with flow or a western blot may confirm previous studies results using different cell lines.

2.3.3 ICAM-1 Expression

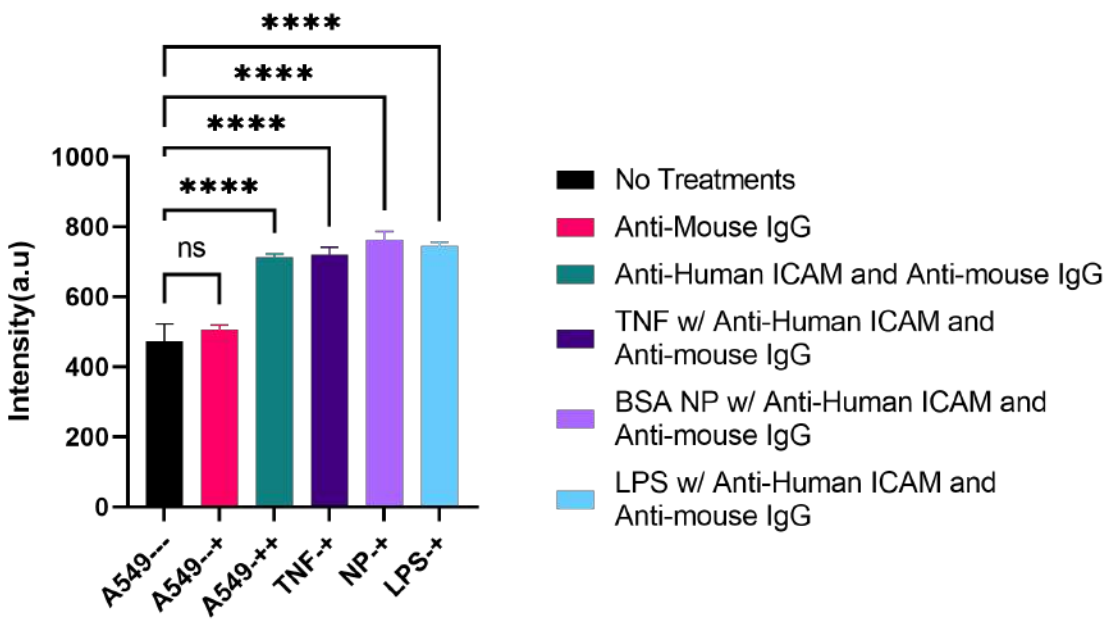

Figure 2.5 ICAM-1 Expression in A549. (n=3, One-way ANOVA, *$p<0.05$, **$p<0.01$, ****$p<0.0001$)

To determine whether ICAM-1 expression was upregulated due to inflammation or nanoparticle treatments an ICAM-1 expression staining test was conducted (Figure 2.5). A549 cells were seeded at ~ 3.0-5.0 x 10^4 cells per well in a 48 well plate. The control were cells with no treatment or antibodies (A549---). The control for non-specific binding of non-specific antibody were cells with no treatment but exposed to a secondary antibody, goat anti-mouse IgG (A549--+). A549 cells with both the primary, mouse anti-ICAM, and secondary antibodies (A549-++). A549 cells with TNF-a stimulation (10ng/ml) and both antibodies (TNF++). A549 cells with BSA

NPs (10ug) and both antibodies (NP++). A549 cells with Lipopolysaccharide (LPS) (5ug/ml) and both antibodies (LPS++). Based on Figure 2.7, A549 cells express similar levels of ICAM-1 receptors for all treatments: TNF-a, LPS, and NPs. The ICAM-1 receptors were not shown to be upregulated in the presence of lipopolysaccharide (LPS). Based on the literature on the upregulation of ICAM-1 receptors in A549 cells, it was expected that LPS stimulation would induce more uptake of ICAM coated nanoparticles[77]. Previous studies have shown that the upregulation of ICAM-1 is dose dependent and time dependent [76]. In Figure 2.7, A549 cells were treated with 5 μg/ml of LPS for 12 hours and then flow cytometry was conducted. If this experiment was repeated, treating cells with 10 μg/ml of TNF- a for 2,4,6, or 8 hours and measuring ICAM-1 expression with flow or a western blot may confirm previous studies results using different cell lines.

2.3.4 Antibody Coating Density Optimization

In human umbilical vein endothelial cells (HUVEC), an ICAM-1 positive and ACE2 positive, the hypothesis was that anti-ICAM coated NPs would have an increased uptake compared to bare NPs and anti-ACE2 NPs because the ICAM-1 receptor is constitutively expressed primarily in endothelial cell lines, providing a target for the ICAM antibodies. Chemical crosslinking was used to stabilize the anti-ACE-2, anti-ICAM-1 and IgG protein coatings, producing covalently bound protein coatings on BSA NPs. Covalent methods to coat proteins onto the surface of protein nanoparticles have been used previously in our lab to create vaccines. To create covalent protein coatings with ACE-2, ICAM-1, and IgG antibodies, the same methods used to create vaccines were adapted. Nanoparticle internalization was measured to determine the optimum amount of protein needed in the coating (Figures 2.6-2.8). From this analysis, the 7 μg/mL anti-ACE2 and 35 μg/mL anti-ICAM-1 protein coatings successfully facilitated increased nanoparticle uptake (Fig. 2.8). Furthermore, uptake results using the 50 and 100 μg/mL protein coatings were similar to the 10 μg/mL antibody coating results, which suggested that the optimization was still necessary (Fig. 2.6-2.7). Due to material constraints, a larger amount of protein coating (>105 μg/mL) was not evaluated. However, 5, 7, 35, and 105 μg/mL antibody coatings were evaluated. Overall, the 7 μg/mL anti-ACE2 and 35 μg/mL anti-ICAM-1 protein coatings were chosen as the covalent coatings because they had the most significant uptake between the different coating densities.

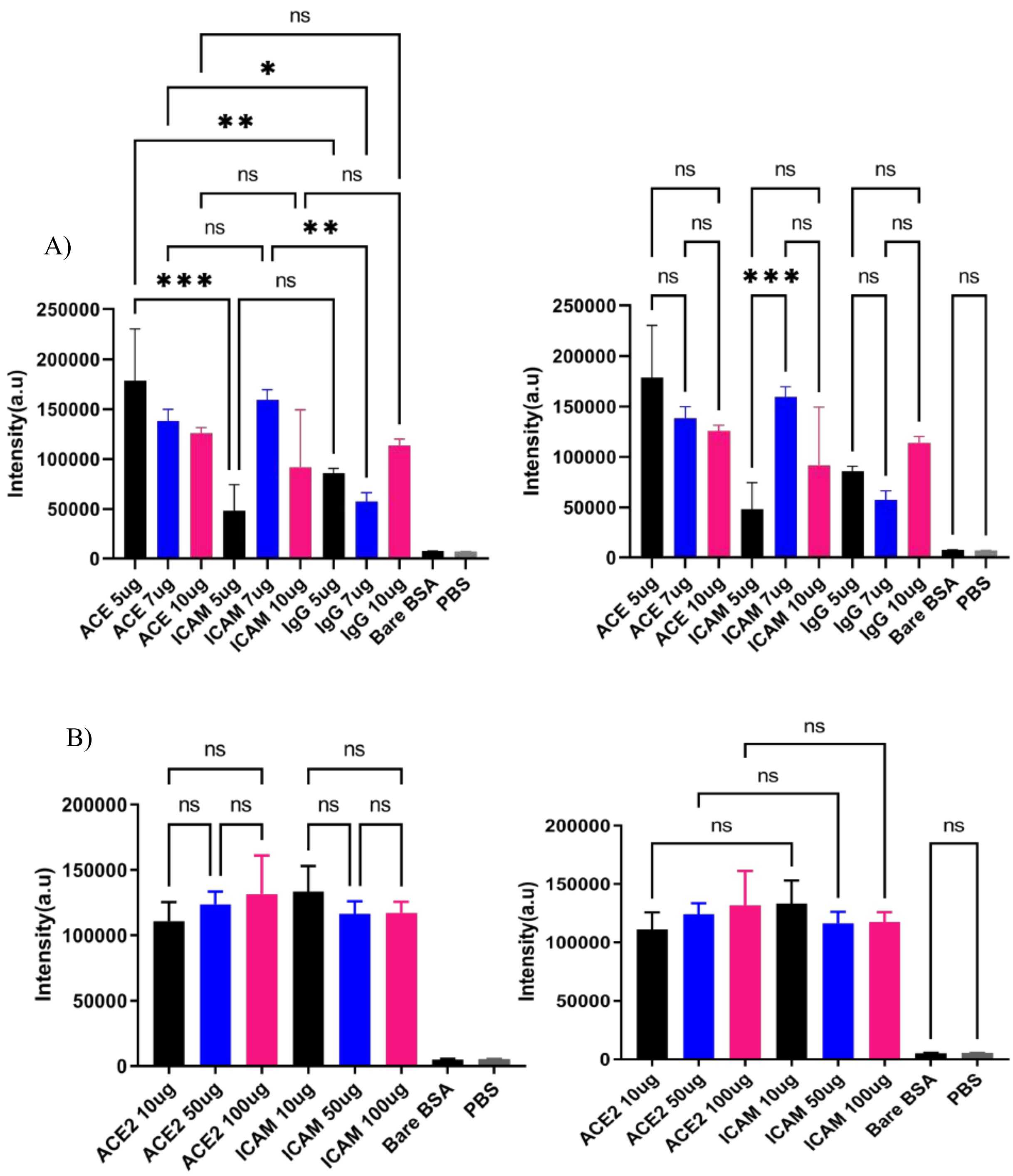

Figure 2.6 Optimization in HUVECs at A) 5ug/ml, 7ug/ml, and 10 ug/ml and B) 10ug/ml, 50ug/ml, and 100 ug/ml coating densities. (n=3, One-way ANOVA, *p<0.05, **p<0.01, ****p<0.0001)

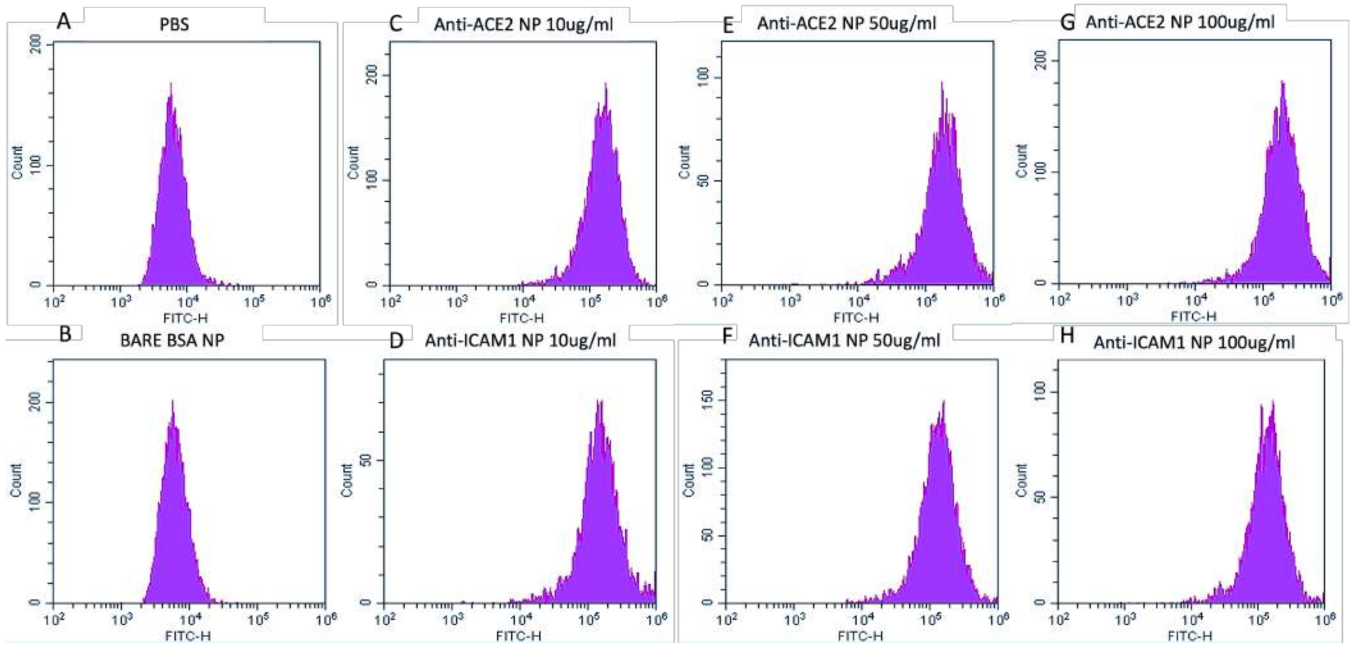

Figure 2.7 Flow cytometry histogram based in Figure 2.6B optimization in HUVECs at 10ug/ml, 50ug/ml, and 100 ug/ml coating densities.

The histograms above in Figure 2.7 display the data from Figure 2.6B. The FIT-H is on the x-axis and the number of events is on the y axis. There is a visible shift in the population between the PBS (control) and Bare BSA NPs compared to the conjugated antibody coatings for 10,50, and 100 ug/ml NPs.

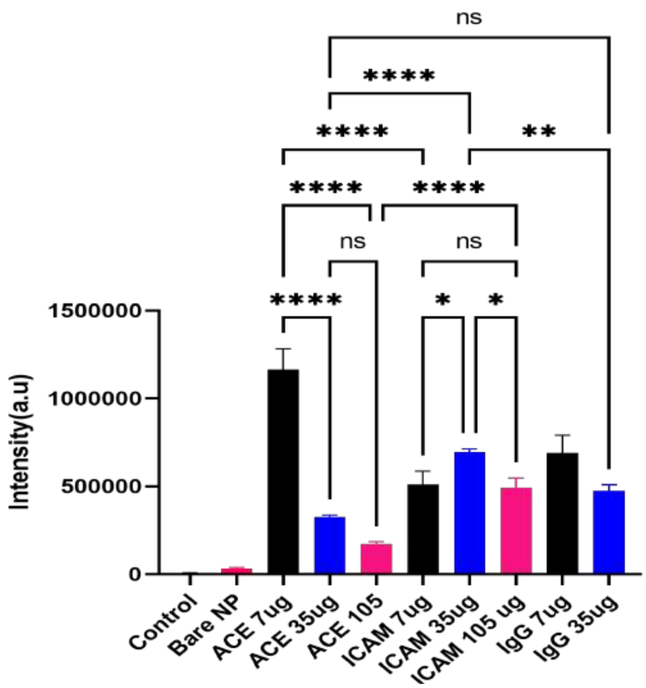

Figure 2.8 Optimization in HUVECs at 7ug/ml, 35ug/ml, and 105 ug/ml coating densities. (n=3, One-way ANOVA, *p<0.05, **p<0.01, ****p<0.0001)

2.3.4.1 Bangs Laboratory Calculation

To further determine the optimum coating density for covalently coated protein nanoparticles, an estimation for amount of protein that would comprise a monolayer of protein was used (Equation 1). Based on Bangs Laboratories covalent coupling protocols for polystyrene microspheres, the calculated value of ~ 4 mg of ICAM1 and ACE2 antibodies were needed to saturate 1 gram of 0.2 μm protein nanoparticles (2ug antibody per 500ug NPs).

$$S = \frac{\left(\frac{6}{\mathrm{rSd}}\right)}{\mathrm{C}} \qquad \text{Equation 1}$$

Where S was the amount of protein required to saturate the surface of the NP, rS was the density of solid sphere (protein density assumed to be 1.33 g/cm^3 based on BSA) [78], d was the mean diameter (μm), and C was the capacity of microsphere surface for a given protein (assumed to be ~ 2.7 mg/m^2 based on MW of ICAM1 and ACE2). Comparing the MW of anti-ICAM1 and anti-ACE2 (90-110 kDa) to that of BSA (66.5 kDa) and IgG (150 kDa), with a capacity value, C, of 3 mg/m^2 and 2.5 mg/m^2 for BSA and IgG respectively. With these parameters, the surface saturation of ICAM1 and ACE2 was approximated[79]. The final number calculated was higher than the *in vitro calculations* for the anti-ACE2 coating (1.4ug antibody per 500ug NPs) and lower than the anti-ICAM1 coating calculated (7ug antibody per 500ug NPs). Ultimately, the optimal protein concentration may be substantially higher (10x) or lower than the monolayer value calculated depending on the activity of the target. Therefore, the flow cytometry data was used to determine optimal protein concentration.

2.3.5 Confocal Microscopy

The combination of nanoparticle surface ligands, size, and cellular interactions with epithelial and endothelial cells affect uptake. Protein nanoparticles with conjugated antibody: ICAM-1, ACE-2, and IgG were incubated, along with uncoated particles, with A549 epithelial cells and endothelial HUVEC cells and internalization was observed by confocal microscopy (Figure 2.5).

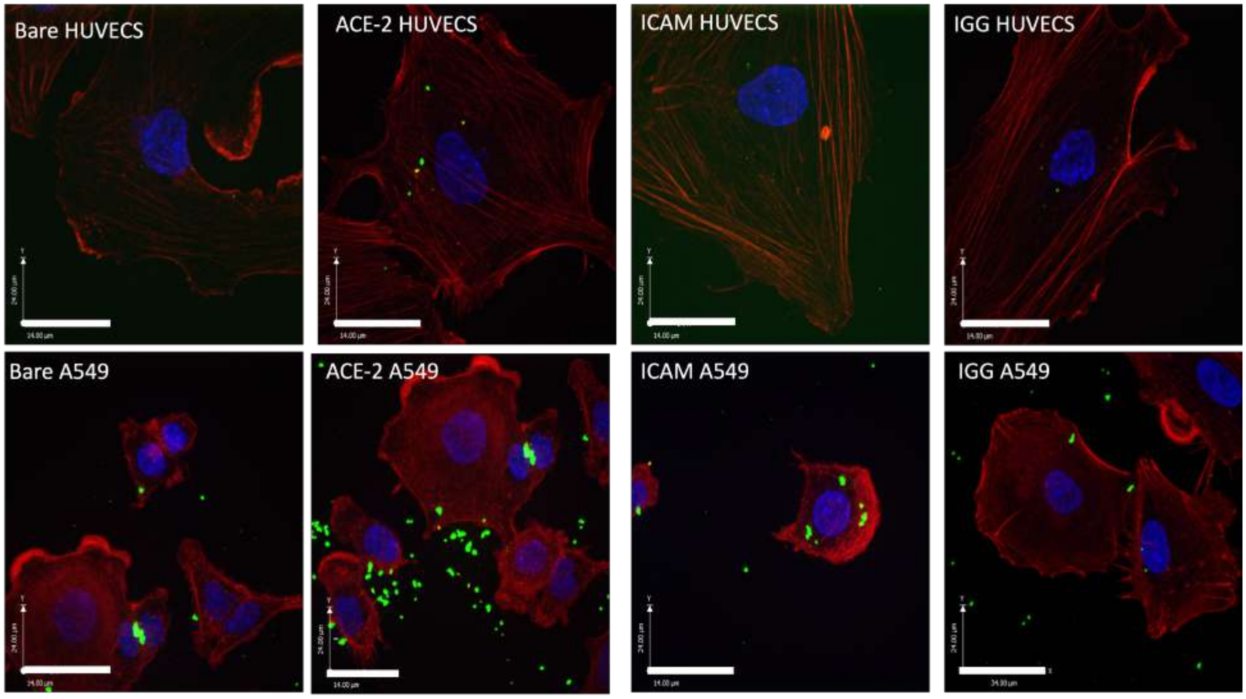

Figure 2.9 Representative confocal microscopy of internalized Bare BSA, ICAM-1 BSA, ACE-2 BSA, and IgG BSA NPs. Fluorescent protein nanoparticles (1 ng/cell), fabricated conjugating BSA protein with Alexa Fluor 488 prior to desolvation, were incubated with A549 and HUVEC cells for 4 hours at 37°C. Images were obtained after NP incubation using a PerkinElmer Spinning Disk Confocal. (Scale bar – 14 µm; nanoparticles – green, A549/HUVEC actin cytoskeleton – red, nuclei - blue)

The cellular uptake profile using HUVEC endothelial cells indicated the highest cellular uptake for anti-ACE2 protein nanoparticles, which is the opposite of what is shown in the A549 cells. Moreover, anti-ICAM1 particles have been shown to have 4x more uptake in A549 cells than anti-ACE2 and Bare NPs. Internalization of anti-ICAM-1 nanoparticles has been confirmed to utilize a unique kinase induced pathway that is distinct from clathrin or caveolin mediated endocytosis[80]. However, the endocytosis pathway that is used by ACE2 is unspecified. Based on the confocal data, there appears to be aggregation of the nanoparticles in the A549 cell line. This aggregation is not present in the HUVEC representative images which implies that cell culture medium may have resulted in surface charge adjustments causing the particles to aggregate.

2.4 Summary

The clinical application of nanoparticles requires specific modifications to achieve targeted delivery. Decorating the surface of nanoparticles with high affinity, specific targeting ligands has been shown to enhance selective delivery of nanoparticles. Furthermore, ensuring optimum coating density for functionality and increased targeting is crucial to minimize nonspecific accumulation in organs and tissues. To maximize specific targeting to the ICAM-1 and ACE-2 receptors, we fabricated and optimized the protein nanoparticles *in vitro* with antibodies (ICAM-1 and ACE-2) at various coating densities. Our analysis revealed distinct changes in uptake in both endothelial and epithelial cells based on the coating density and the receptor-ligand interaction. We demonstrated methods to modify the surface of nanoparticles with conjugated antibodies and characterized the nanoparticles. Moreover, our findings report that BSA nanoparticles crosslinked with antibodies increase cellular uptake in HUVEC and A549 cell lines. The challenge of *in vitro* studies is that it rarely translates to the biological environment of *in vivo* studies[81].

CHAPTER 3. IN VIVO BIODISTRIBUTION OF PROTEIN NANOPARTICLES

3.1 Introduction

With an increasing number of proteins used as therapeutic agents, the efficacy of these proteins is usually impaired due to poor delivery in the body, limited targeting to diseased organs and tissues, and intracellular delivery of cargo [82]. These challenges can be improved by conjugating these therapeutic proteins with nanoparticles to increase affinity for specific tissues and delivering therapeutic proteins intracellularly. Surface density of the targeting ligand on the nanoparticle and the bulk concentration in the case of ICAM-1 targeted nanocarriers severely improves targeting specificity and efficiency[82]. Targeting ICAM-1 receptors induces transport of nanoparticles across cellular barriers and into lysosomes[83], [84]. However, the administration of targeted nanoparticles intravenously will not prevent accumulation of nanoparticles in other, non-targeted tissues.

Previous research on nanoparticle biodistribution *in vivo* has determined that nanoparticles preferentially accumulate in the liver, spleen, and kidney [47], [85], [86]. The liver functions to remove foreign material from the blood stream and the kidneys filter waste and nutrients, receiving substantial blood flow, which explains the nonspecific accumulation of nanoparticles in these organs which in confirmed in literature[87]–[89]. There is an inverse relationship between serum proteins and clearance time in the blood. The more extensive serum protein opsonization and interactions, the quicker the particles are cleared[90]. In addition, the endothelial targeted nanoparticles would specifically accumulate in the liver with its abundance of endothelial cells. The spleen is comprised of endothelial cells called the splenic sinuses which would interact with anti-ICAM1 and anti-ACE2 coated nanoparticles. In addition, the macrophages of the spleen tend to selectively internalize particles between 100-200nm. There is evidence that demonstrated that particles larger than 200nm are incapable of being internalized by endothelial cells and will be retained and internalized by pulp macrophages and destroyed [91]. This preferential accumulation presents a barrier to clinical applications, especially for nanomedicines administered intravenously.

There are a few methods that have been utilized in literature to assess biodistribution of nanocarriers (NCs) *in vivo*. The range of techniques to evaluate biodistribution of nanoparticles includes, but are not limited to histology, electron microscopy (EM), indirectly measuring drug concentrations, liquid scintillation counting (LSC), and magnetic resonance imaging (MRI), radiolabeling, and optical imaging [92]. Histology has the advantage of being a cost-effective method that allows for the study of large tissue sections, especially within a cellular context. However, low resolution for fluorescent microscopy, limited tissue sections, and human error and labor are disadvantages to this technique. Electron microscopy is predominantly used *in vitro* but has high resolution; allowing for visualization of accumulated nanoparticles. EM is a very expensive technique and incapable of evaluating large tissue sections. LSC requires that particles are labeled with isotopic markers before administration, but has the advantage of being a sensitive, specific, and quantitative technique that has been used to label anti-ICAM-1 liposomes before being administered intravenously in rats with inflammation[93]. This technique is laborious and does not provide information regarding specific accumulation of particles in tissues. Measuring drug concentration in tissues assumes that the particles make it to the tissues before releasing its cargo; however, it does not consider the premature release from the nanoparticles and the biodistribution of the drug. Furthermore, this research did not incorporate a protein drug as cargo within the particle. Optical (fluorescence) imaging is another method of visualizing accumulation and biodistribution of nanoparticles in organs and tissues[94]. This technique utilizes equipment such as the *In Vivo* Imaging System (IVIS) and has the advantage of being direct, non-invasive, and simple to conduct. Imaging can be performed in real-time which allows biodistribution to be assessed over many time points with high sensitivity and resolution. Limitations of this technique are the limited tissue penetration, tissue autofluorescence, and the inability to visualize individual particles[95], [96]. For the *in vivo work* discussed in this chapter, IVIS imaging was used to assess nanoparticle biodistribution in mice.

In this chapter, nanoparticles were fabricated with covalent targeting ligands with specificity for the ICAM-1 and ACE-2 receptors at an optimized density, based on Chapter 2 analysis, and administered to healthy balb/c mice to study their biodistribution. Mouse serum albumin (MSA) was used for the mouse experiments instead of bovine serum albumin (BSA) to incorporate a native protein found in mice as the carrier protein. Based on previous *in vivo* studies, it was expected that nonspecific organ accumulation in the liver, spleen, and kidneys would be found, and the implications of protein corona may affect clearance time and cell interaction[97]. This work assesses the biodistribution and blood circulation time of optimized targeted particles in healthy mice to identify any preferential accumulation in the lungs using optical imaging technology. Based on the *in vitro* studies, it is expected that coated nanoparticles will target endothelial receptors. More specifically, due to the presence of endothelial cells in the lungs[98]–[100], the anti-ICAM1 and anti-ACE2 particles should target the lungs with more specificity than uncoated nanoparticles.

3.2 Methods

3.2.1 Mouse Serum Albumin Nanoparticle

Mouse Serum Albumin (MSA) nanoparticles were fabricated using a desolvation method (Sigma-Aldrich). 10 mg of MSA, not endotoxin free, was dissolved in 1 mL endotoxin free water at pH 9.0 (18.2 MΩ·cm). Then, 400 μL of acetone desolvent was added dropwise at 1 mL/min to 100 μL of MSA protein solution. Next, 3,3'-dithiobis (sulfosuccinimidyl propionate) (DTSSP) was added in a molecular ratio of 2.2 molecules lysines present in the protein to one molecule DTSSP and the solution was mixed on a stir plate at 700 rpm. After mixing for one hour, the protein solution was centrifuged at 10,000 x g for 10 minutes. The supernatant was removed, and the pellet was resuspended in 0.5 mL of sterile medical grade phosphate buffered saline (PBS, pH 7.4). The nanoparticles were sonicated twice on ice for 1 minute, with 2 second pulses at 60% amplitude. The nanoparticles were then centrifuged for 5 minutes at 700 x g at 4 ˚C and the supernatant was collected while the pellet was discarded. This centrifugation step was repeated twice.

3.2.2 Nanoparticles Characterization

Protein nanoparticle size distribution were determined using Dynamic Light Scattering (DLS) with a Malvern Zetasizer Nano ZS90. Each sample was measured 3 times and each measurement had 10 runs with a dispersion medium of PBS. Protein nanoparticle concentrations were assessed using a BCA Assay according to the manufacturer's instructions (Thermo Scientific, Waltham, MA).

3.2.3 Alexa Fluor-647 Fluorescent Nanoparticle

AlexaFluor 647 5-SDP Ester (Thermo Fisher Scientific) was dissolved in DMSO according to the manufacturer manual. 10 mg MSA and Alexa Fluor 647 dye were mixed at a ratio of 0.4 mg of protein to 1 µL of dye in 1 M sodium bicarbonate solution (pH=8.3) and stirred continuously at room temperature for 1 hour. After conjugation, excess dye was removed through filtered centrifugation cycles using a 10 kDa molecular weight cutoff filter buffer exchanged to phosphate-buffered saline (PBS, pH 7.4). Degree of labeling and the final protein concentration was measured using the fluorescent dye labeling settings on a NanoDrop 2000. To make fluorescent NPs, the nanoparticle fabrication and characterization procedures described above were used to fabricate fluorescent protein nanoparticles. 15% soluble MSA conjugated with Alexa Fluor 647 was supplemented into the MSA solution.

3.2.4 Covalent Protein Coatings

Anti-ACE2 Coatings: The ACE-2 targeting antibody used was monoclonal (CL4013) mouse IgG recognizing mouse, human, and rat ACE-2 (Thermo Fisher Scientific). 500 µg of MSA NPs, 7 µg/mL anti-ACE2 antibody (the volume of the solution was adjusted to 200 µL with PBS), and 0.1 mg of DTSSP were mixed in a 1.5 mL eppendorf tube. Samples were reacted for 12 hours at 4°C under constant stirring of 1200 rpm. Once the reaction was complete, 25 µL of 1 M Tris base (pH = 7.6) was added to the nanoparticles to quench unreacted DTSSP for 10 minutes on a stir plate. Nanoparticles were then collected using centrifugation (15,000 x g, 10 mins, 4°C) and the pellets were resuspended in 200 µL of sterile PBS. The nanoparticles were sonicated twice on ice for 1 minute, with 2 second pulses at 60% amplitude. Nanoparticle concentration was assessed using BCA assay and the size distribution was measured using DLS.

Anti-ICAM1 Coatings: The ICAM-1 targeting antibody used was monoclonal (CD54/YN1) rat IgG recognizing mouse ICAM-1(Thermo Fisher Scientific). 500 µg of MSA NPs, 35 µg/mL anti-ICAM1 antibody (the volume of the solution was adjusted to 200 µL with PBS), and 0.1 mg of DTSSP were mixed in a 1.5 mL eppendorf tube. Samples were reacted for 12 hours at 4°C under constant stirring of 1200 rpm. Once the reaction was complete, 25 µL of 1 M Tris base (pH = 7.6) was added to the nanoparticles to quench unreacted DTSSP for 10 minutes on a stir plate. Nanoparticles were then collected using centrifugation (15,000 x g, 10 mins, 4°C) and the pellets were resuspended in 200 µL of sterile PBS. The nanoparticles were sonicated twice on ice for 1 minute, with 2 second pulses at 60% amplitude. Nanoparticle concentration was assessed using BCA assay and the size distribution was measured using DLS.

3.2.5 Endotoxin Measurement

Protein nanoparticle endotoxin content was quantified using the Genscript ToxinSensor Chromogenic LAL Endotoxin Assay according to manufacturer's guidelines. The endotoxin threshold for subsequent mice experiments were a maximum drug dose of 0.200 mL and 1 EU per mL of drug according to the United States Pharmacopeia (USP) limits for small animals[101].

3.2.6 Biodistribution Experiment

Mice in all experiments were 6–8-week-old Balb/c male and female (37M/37F). Balb-C mice were ordered at least a week in advance and given time to adjust to the environment at least three days before experiment. The mice were fed a non-fluorescent alfalfa free chow.

3.2.6.1 Intravenous (IV) Administration

To prepare for IV administration, the oxygen supply was turned on for the procedure room. Prior to bringing the mice to the procedure room, the working space was set up. The heating block was turned to 107°F. Next, the isoflurane level was verified, and the oxygen line connected. The anesthesia chamber was lined with paper towels and connected to the anesthesia mask. The anesthesia chamber was turned on with the isoflurane unit set to 5% and a flowrate to 1000 ml/min. The mice were checked out of the housing rooms and brought to the procedure room. One mouse at a time, they were placed into the anesthesia chamber. After 15 minutes, the isoflurane was reduced to between 2.5-3% and a flow rate of 200 ml/min. Then, the mouse was placed on its back on the heating block. Both sides of the mouse's face and neck were shaved. Nair was added liberally, allowed to sit for 1-2 minutes, and removed with a dry gauze. Then, a 1 ml syringe was placed under the neck of the mouse and the nose tilted down to lift the chest upwards. The arms of the mouse were taped down and across the chest to pull the skin taught (with enough room for the mouse to breathe). Next, using an uncapped insulin needle, 200 µL of sample for administration was loaded. The syringe was tapped to remove any air bubbles. Next, the jugular vein was located, and the needle was inserted angled downward, and towards the outer-ear into the chest with the bevel facing up. Once the needle was positioned, the syringe was pulled back slightly. If blood was not drawn, then adjustments were made. If blood was drawn, nanoparticles were administered until syringe was empty and the plunger was pulled back until ~10 µL of blood was collected and then removed. Finally, the isoflurane was turned off and the mouse was given time to recover before returning to its cage. Injections were documented as unsuccessful or missed if a "bubble" was observed during the injection or if blood was not drawn back into the syringe after injection. These missed injections were not used in further *in vivo* analysis.

3.2.6.2 Blood Sampling

To prepare for blood collection, the same steps from above for IV administration were followed. After the allotted time for each group, each mouse was placed in the anesthesia chamber and then placed on the heating block and prepped for blood collection. After 15 minutes, the isoflurane was reduced to between 2.5-3% and a flow rate of 200 ml/min. A 1 ml syringe was placed under the neck of the mouse and the nose was tilted down to lift the chest upwards. The arms of the mouse were taped down and across the chest to pull the skin taught (with enough room for the mouse to breathe). Next, an insulin needle was uncapped and primed, syringe plug pulled back and forth to loosen. To remove any bubbles and push air out, the syringe was tapped lightly at the end. Next, the jugular vein was located, and the needle was inserted angled downward, and towards the outer ear into the chest with the bevel facing up. Once the needle was positioned the syringe was slightly pulled back to ensure that the needle was in the jugular vein. The plunger was pulled back until ~200 µL of blood was collected and then removed. Then the tape was removed, and isoflurane turned off and mouse placed in euthanasia chamber.

3.2.6.3 Euthanasia

The CO2 tank was turned on and pre-label bags were prepped for mice to be placed in after euthanasia and organ collection. The CO2 chamber was lined with paper towels and mice were placed in the CO2 chamber for 5 minutes.

3.2.6.4 Biodistribution Study

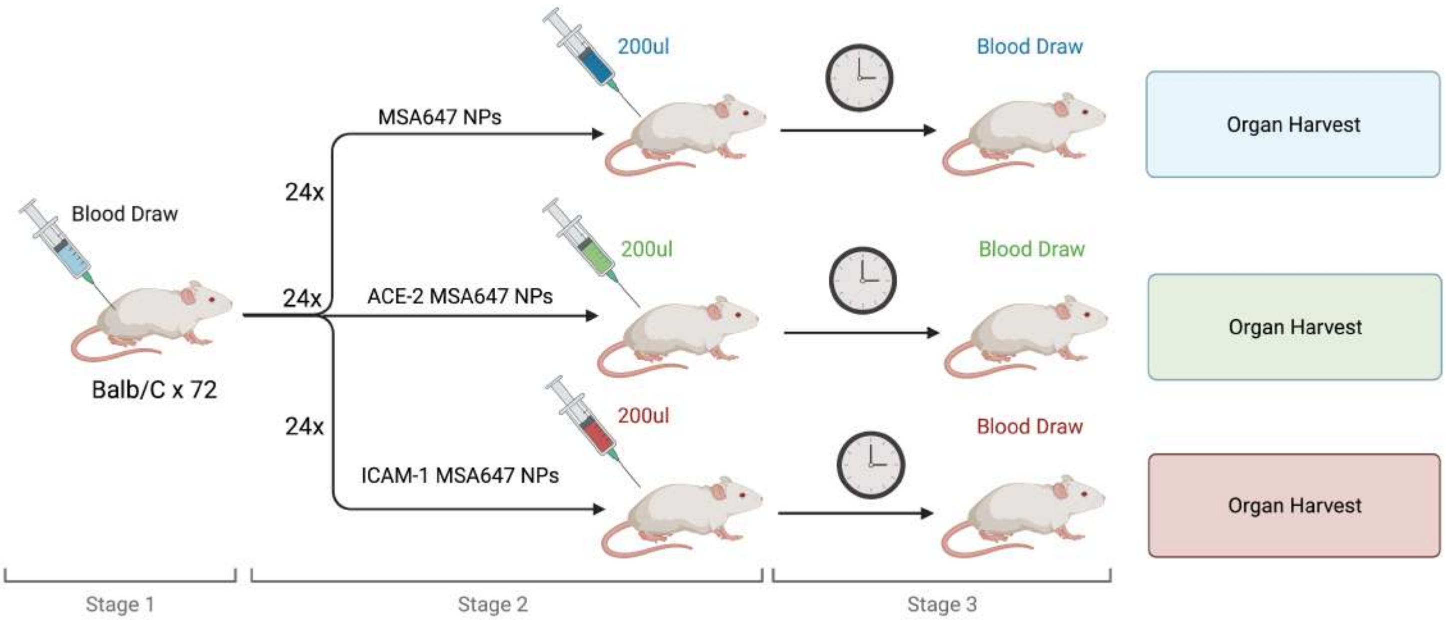

Figure 3.1 Schematic of administration of nanoparticles and blood collection (BioRender). For all three groups of mice (MSA647, ACE2, and ICAM1), there was an initial blood draw (before 43.2 µg dose of nanoparticles were administered) for all mice in the 2hr,6hr, and 24hr timepoints. Once the nanoparticles were administered and the allotted time (2hr,6hr,24hr) was met, a terminal blood draw was taken from each mouse. Then, the organs were harvested and prepped for IVIS.

3.2.6.5 IVIS Imaging

After logging into the IVIS imaging software, the instrument was initialized until the camera chilled to -90 °C. The software turned from red to green when ready. “Imaging wizard” was selected, followed by “Fluorescence.” Then, the filter pair was chosen (AF647) and Field of View was selected as “B”. Subject height: 0.5cm and a binning if medium was selected. Then, the sequence was acquired using Radiant Efficiency. Region of Interest (ROI) tools were used to measure fluorescence in each organ.

3.2.6.6 Blood Processing

Blood samples (20ul) were taken from the mice initially and at the terminal time points (2,6, or 24 hours after injection). The samples were then analyzed by a Biotek Synergy 2 Microplate plate reader.

3.3 Results and Discussion

3.3.1 Protein Nanoparticle Fabrication and Characterization

Nanoparticle size is one of the most important physiochemical properties that influence the interaction between the nanoparticle and the cell. Therefore, it is imperative that the fabricated protein nanoparticles are between 100-200nm in size. There were challenges initially in fabricating MSA nanoparticles that resulted in poor stability, larger size distribution, and polydispersity index (PDI). However, adjusting the pH of the solvent from 4 to 9 made a huge difference in the nanoparticle size. I found that it was important to prepare the protein nanoparticles in unbuffered aqueous medium due to the buffer ions influence on reducing surface charge density, leading to attraction and fusion between particles and increasing the particle size [[102]. Using Dynamic Light Scattering (DLS), fabrication bare MSA and coated MSA nanoparticles were confirmed to be 200nm in size (Figure 3.2). Table 3.1 depicts the diameter of the protein nanoparticles used for the biodistribution experiment.

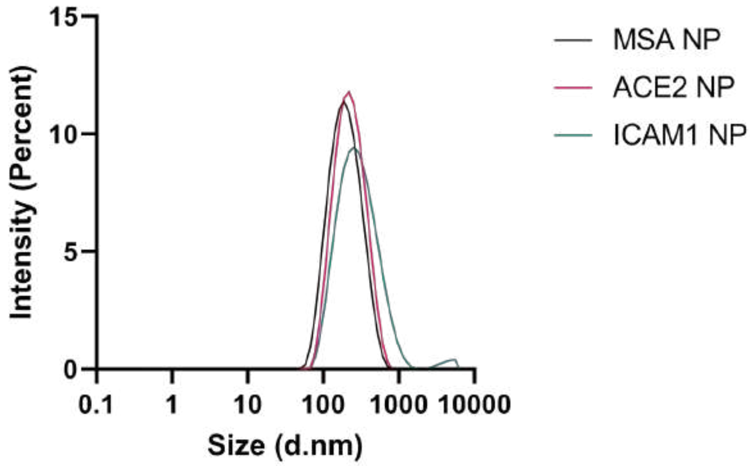

Figure 3.2 Characterization of MSA NPs. Size distribution overlay of BSA NPs with conjugated ACE-2 or ICAM-1 antibodies at 7 ug/ml and 35ug/ml respectively using DLS

Table 3.1: Summary of Bare MSA NP, anti-ICAM-MSA NP, and anti-ACE2-MSA NP Size using dynamic light scattering (DLS) (d.nm)

Sample[a]	D (nm)[b]	STD.DEV	PDI[c]	STDDEV
MSA NP Core	174.0	1.8	0.15	0.034
7 µg/mL ACE2	200.4	0.8	0.12	0.004
35 µg/mL ICAM1	246.6	3.5	0.27	0.021

[a] n=3 independent batches of nanoparticles; [b] hydrodynamic diameter; [c] polydispersity index

3.3.2 *Biodistribution Results*

3.3.2.1 Biodistribution Study

To assess biodistribution in healthy mice, 43.2 µg of 15% A647-labelled MSA NP with optimized anti-ACE2, anti-ICAM- 1 or no coating were injected via jugular vein (Figure 3.2). Terminal blood samples were taken at 2, 6, and 24 hours. At 2, 6 and 24 hours, animals were sacrificed, and major organs (lungs, liver, spleen, heart, and kidneys) were collected, weighed, and imaged by IVIS. Blood fluorescence was quantified by fluorimetry. Each group (n=4-8) were successfully given a dose of nanoparticles via jugular injection. Animals that did not receive full injections or mice that passed away, were not included in quantification analysis. It was expected that ACE2, and CAM-1 targeted NPs will accumulate in the lungs to a greater extent than non-targeted. Based on the *in vitro* studies, we expected that nanoparticles would target the lungs and the liver with more specificity for the lungs with the anti-ACE-2 coated nanoparticles.

The IVIS images qualitatively showed more fluorescent signaling in the lungs for the coated nanoparticles compared to the uncoated particles after 2 hours (Figures 3.3). However, when quantified, there was no statistical difference between targeted and untargeted particle signal in the lungs or liver (Figure 3.6). It was expected that targeting would accumulate in the liver and spleen, as there are receptors for ICAM-1 and ACE-2 present. In addition, nanoparticles without additional coatings tend to accumulate in these organs. There are ICAM-1 receptors in the spleen, but expression of ACE-2 is reported to be low in the spleen [[103], [104]. The IVIS data at 2hr and 6hr were very similar for the liver and spleen, though no obvious signal was detected in the lungs (Figure 3.3 and 3.4). However, the 24 hr. results show little to no fluorescence in any organs and blood fluorescence was nonexistent after 2hr (Figures 3.7). This short circulation time was expected due to previous evidence that nanoparticles clear the blood after minutes[105], [106]. Remaining IVIS mice images are in the Appendix, A.1-A.3.

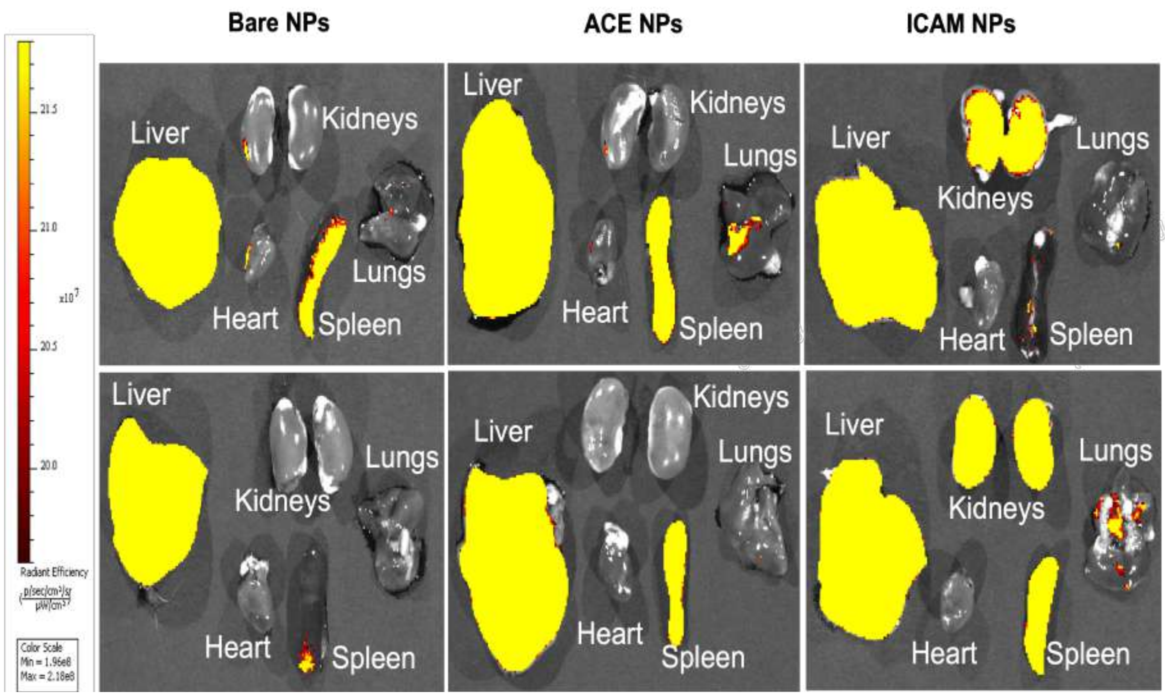

Figure 3.3 This is a 2-hour representative *ex vivo* imaging of Bare NPs signal using IVIS (A) ACE NPs signal and (B) ICAM NPs signal (C) of organs (left to right respectively liver, heart, kidney, spleen, and lung). The unit of radiant efficiency is [(p/sec/cm^2/s)/(μW/cm 2)].

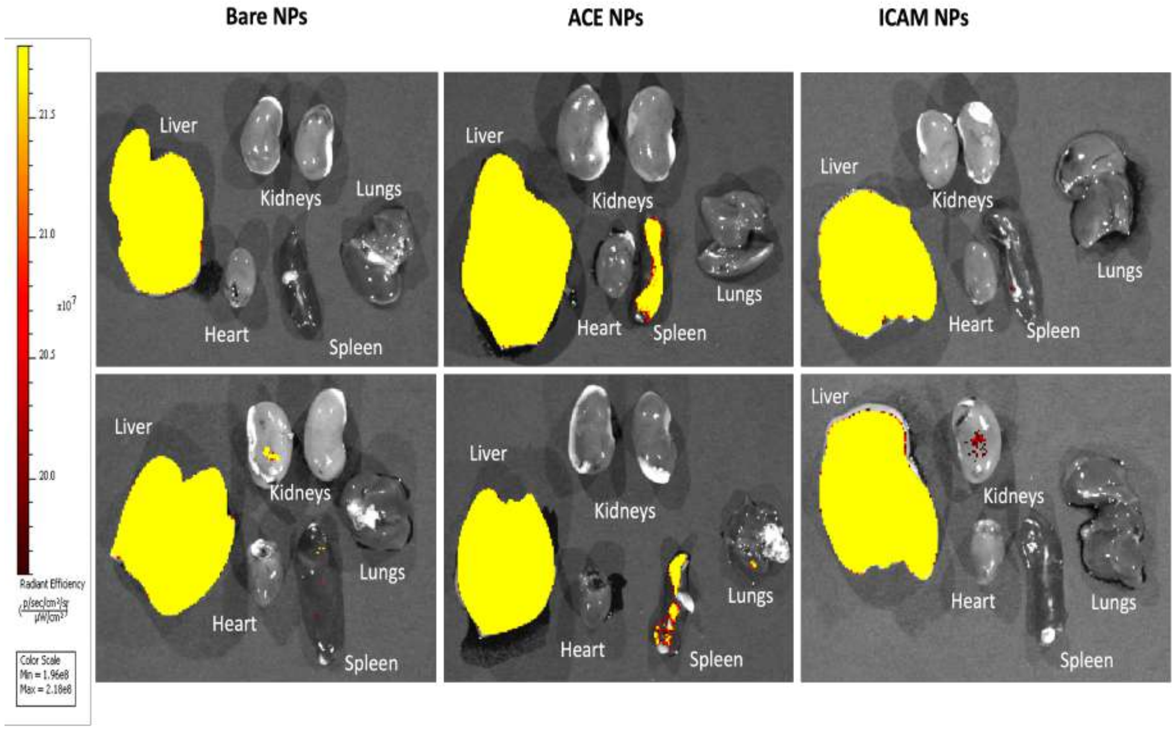

Figure 3.4 This is a 6-hour representative *ex vivo* imaging of Bare NPs signal using IVIS (A) ACE NPs signal and (B) ICAM NPs signal (C) of organs (left to right respectively liver, heart, kidney, spleen and lung). The unit of radiant efficiency is [(p/sec/cm^2/s)/(µW/cm 2)].

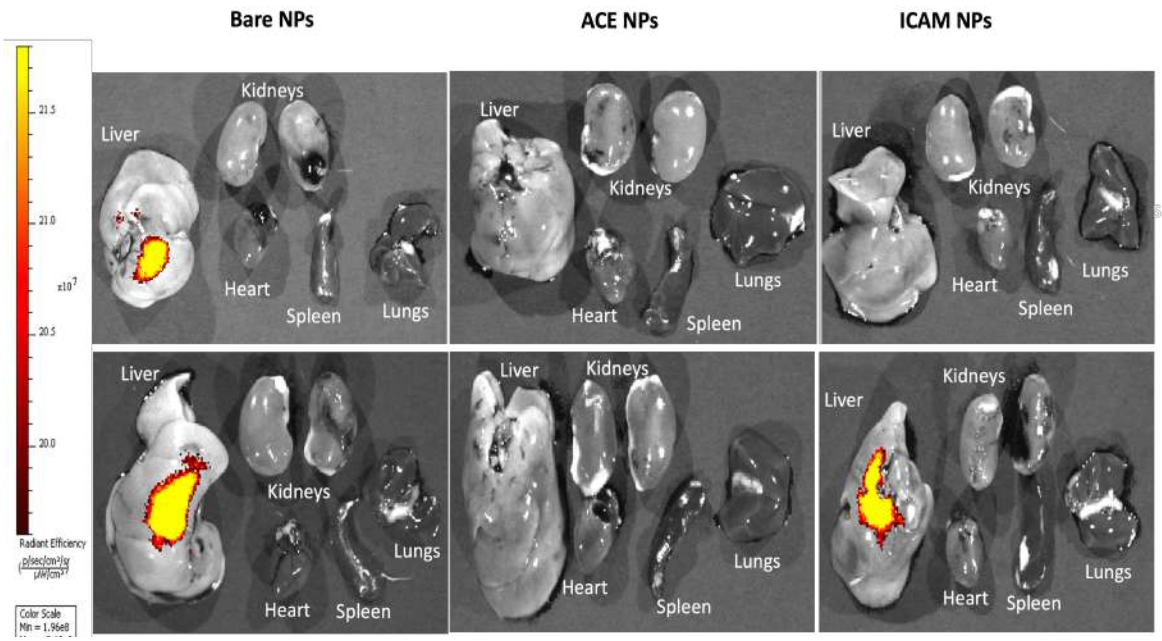

Figure 3.5 This is a 24-hour representative *ex vivo* imaging of Bare NPs signal using IVIS (A) ACE NPs signal and (B) ICAM NPs signal (C) of organs (left to right respectively liver, heart, kidney, spleen and lung). The unit of radiant efficiency is [(p/sec/cm^2/s)/(µW/cm 2)].

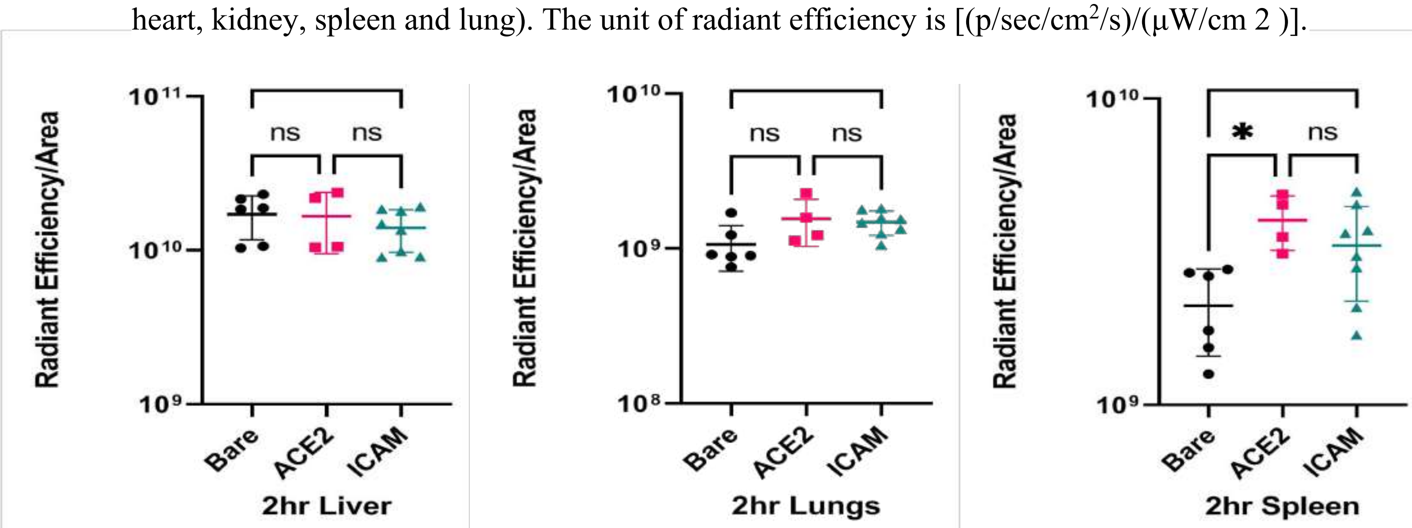

Figure 3.6 Quantification of organ fluorescence after 2 hours using IVIS (*$p<0.05$, **$p<0.01$, ****$p<0.0001$). Data depicted are fully administered protein nanoparticle doses based on observed administration to the jugular vein. The unit of radiant efficiency is [(p/sec/cm^2/s)/(µW/cm 2)].

Altogether, neither coating (Anti-ACE-2 or Anti-ICAM-1) showed increased targeting to highly vascularized tissue (i.e., lungs). Research has shown that increased accumulation in the lungs was achieved when upregulating ICAM-1 with LPS administration[107]. However, the mice did not have induced inflammation, so ICAM-1 targeting inflamed endothelium may be improved in a disease model that incorporates vascular inflammation. The quantification of organ fluorescence shows that there is a statistical difference between the anti-ACE-2 coating targeting to the spleen than bare MSA nanoparticles at 2 hours, but there is no significance between the anti-ACE-2 and anti-ICAM-1 NPs in the spleen or between non-coated NP and anti-ICAM-1 NPs which can be explained by the, minimized error bars, due to the smaller group size of the (n= 4) anti-ACE2 group compared to the larger (n=8) anti-ICAM group. These results highlight the challenges associated with intravenous delivery of nanoparticles to target cells and lack of correlation with *in vitro* data, a common situation. Based on these findings, future studies need to examine new or different strategies of administering coatings to tune organ and tissue delivery for better control in navigating through the circulatory system. It is possible that increasing particle dose or coating density, modifying particles with polyethylenglycol (PEG) to decrease opsonization and increase circulation[105], and delivering nanoparticles directly to the lungs via aerosol delivery will show more targeting to the lungs. Another explanation for the lack of targeting to the lungs, is that the very quick clearance did not allow for many "passages" through the body, so the particles didn't get many chances to bind their target as they would if they were circulating longer.

Once injected into biological environments, nanoparticles undergo significant modifications through interactions with biological fluid that control nanoparticle delivery to organs, tissue, and cells[108]–[111]. Upon administration of the nanoparticles, biomolecules such as proteins from plasma, swiftly adsorb onto the nanoparticles surface, creating a corona of proteins on the nanoparticle. These absorbed proteins can either improve nanoparticle stability or destabilize the nanoparticle through charge neutralization which causes aggregation [112], [113]. Protein corona formation unpredictably changes the surface characteristics of the nanoparticle and influences the *in vivo* circulation, biodistribution, and bioavailability of nanoparticles by altering the interactions with cells[114], [115]. It is important to note that protein corona can contradict predicted *in vitro* results by initiating premature nanoparticle clearance and biodistribution due to the accumulation of proteins altering nanoparticle surface properties. It should be noted that during *in vitro* experiments, there was corona present, but from fetal bovine serum. The presence of hydrodynamic forces *in vivo* increases the amount of protein adsorption on nanoparticles compared to *in vitro* studies [72]

3.3.2.2 <u>Blood Fluorescence</u>

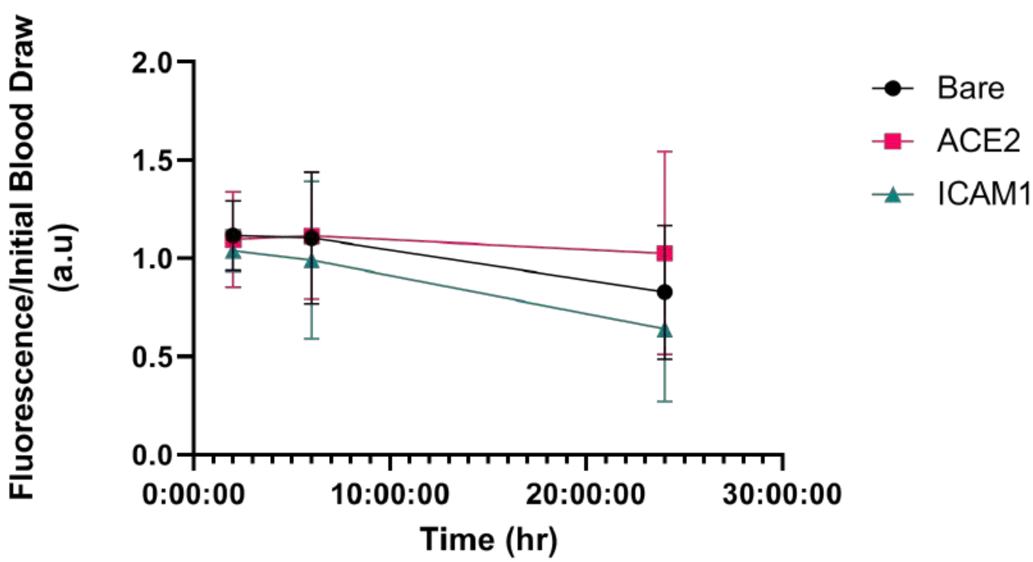

Figure 3.7 Quantification of Blood Fluorescence using a Biotek Synergy 2 Microplate plate reader. Based on the initial and final blood collection of the mice in the three experimental groups (Bare, ACE2, ICAM1) over time (2hr, 6hr, and 24hr). The data depicted are fully administered protein nanoparticle doses based on observed administration to the jugular vein.

The data in Figure 3.7 is normalized based on determining the ration between the initial and final blood fluorescence for each "successful" administration. The ratio is around 1 for all the time points which proves that there was similar fluorescence signal before administering the particles (initial blood draw) and after administering the particles (final blood draw); 2,6, and 24 hours later. Previous research has shown that administering doses less than 1mg (50 μg/g tissue), the half-life of the nanoparticles in blood circulation is around 1-1.5 minutes[105]. Therefore, it was expected that the fluorescence in the blood after administering a 43.2 μg dose of nanoparticles would not be detectable after 2 hours. If this biodistribution study was repeated, including 30-minute, 1 hour, and 4-hour timepoints would be recommended.

3.4 Summary

Intravenous delivery often suffers the effect of opsonization or macrophage uptake barriers that can significantly hinder the ability of nanoparticle delivery *in vivo.* Nanomedicine has proven promising in preclinical trials; however, understanding the distribution of nanoparticles when administered intravenously *in vivo is* crucial to facilitate translation to clinical applications. When considering the preferred method of nanoparticle delivery, particularly when targeting the lungs, intravenous injection is the most common[107], [116]. We have engineered 3 different protein nanoparticles using MSA with conjugated antibodies to target endothelial cells. We have demonstrated that improving the specificity of nanoparticles using coatings such as anti-ACE2 and anti-ICAM-1 may improve uptake in vitro, but the combination of blood shearing, protein corona, and other effects negated differences *in vivo*.

CHAPTER 4. CONCLUSION AND FUTURE WORK

4.1 Conclusions

This defense assessed the *in vitro* uptake and *in vivo* biodistribution of protein nanoparticles with various targeting ligand proteins. This work investigated the specificity and delivery of ACE-2 and ICAM-1 antibodies engineered as coatings on albumin protein nanoparticles. While in vitro cell studies demonstrated targeting, it was established that protein nanoparticles preferentially accumulate in the liver and spleen during intravenous administration without targeting vascularized tissues like the lungs. These studies corroborate previous understanding of nanoparticles delivery for intravenous administration. They motivate different targeting approaches or routes of administration in future work to achieve the delivery goals *in vivo*.

4.1.1 Protein Nanoparticle Characterization and Uptake

Chapter 2 explores the fabrication of different coatings on nanoparticles made from proteins, determining the optimal coating density for increased cellular uptake. We have engineered these coatings to bestow the nanoparticles with different surface ligands to improve targeting to endothelial tissues delivered intravenously and epithelial cells delivered via other routes. We characterized protein nanoparticle size and concentration with different ligands and unmodified using both bicinchoninic acid assay (BCA) and dynamic light scattering (DLS) analysis. In general, nanoparticles with higher coating densities (> 50 ug/ml) showed no increase in uptake by epithelial and endothelial cells in the presence of anti-ICAM-1 and anti-ACE-2 coated nanoparticles. The cellular uptake by A549 and HUVEC cell demonstrates the striking differences between coated and non-coated nanoparticles. Ultimately, proving that coated nanoparticles demonstrate statistically significant increases in uptake compared to uncoated nanoparticles. While the coated nanoparticles particles showed promise *in vitro*, further tailoring the surface of the nanoparticles and the delivery route should be evaluated to improve *in vivo* conditions.

4.1.2 Nanoparticle Biodistribution

Intravenous delivery provides a rapid response and bioavailability. However, this route faces the challenges of systemic circulation that may hinder therapeutics from being delivered[117]. One challenge is reticuloendothelial system (RES) uptake, which consists of phagocytic cells that clear particles and foreign material from the body. To improve delivery, nanoparticles have been modified with antibodies to improve cellular uptake and increase endothelial cell interactions. New methods of direct pulmonary delivery using dry powder formulations containing nanoparticles have shown promise; however, particle sizes would need to range between 1 and 5 µm to be inhaled into the lungs and incorporated into a carrier matrix[118]. Oral delivery of nanoparticles to the lungs has not been promising[119]. Currently, intravenous administration for nanoparticle administration has been the most used method[120]–[122].

In Chapter 3, we assessed the accumulation of protein nanoparticles with anti-ICAM-1 and anti-ACE-2 antibody coatings in the liver, spleen, kidneys, lungs, and heart. Many nanoparticles have been delivered through the intravenous route. However, little work has been done utilizing protein nanoparticles with targeting ligands to intravenously target endothelial cells. Using the same nanoparticles with ligands as the *in vitro* work in Chapter 2, we were unable to show increased targeting to the lungs. However, the mice did not have induced inflammation, so ICAM-1 targeting inflamed endothelium may be improved in a disease model. While these coatings biased uptake *in vitro*, it is very possible that the combination of blood shearing, adsorbed serum protein corona, rapid clearance, and other effects negated differences *in vivo*. Lastly, as expected for nanoparticles without PEG or some other kind of stealth coating, there was no detectable signal in the blood at any of the time points.

4.2 Future Work

4.2.1 In vivo intravenous delivery AvrA-MSA647 nanoparticles

ICAM-1 targeting would be more effective in inflamed environments. Therefore, using the same fabricated and optimized nanoparticles from this research, which accumulated in the liver and spleen, may be effective in reducing systemic inflammation. To test the ability of anti-ACE-2 or anti-ICAM-1 coated AvrA- MSA NP to suppress systemic inflammation, a murine cecal ligation and puncture model (CLP), a commonly used method for evaluation of overwhelming systemic inflammation should be assessed[123]. The CLP model is systemic and not specific to the lungs. Using anesthetized mice, this method involves opening the abdomen and using a suture to tie off a section of the cecum, followed by controlled perforation of the ligated region. This allows escape of fecal material into the peritoneum and rapidly developing systemic inflammation, including vascular and pulmonary injury. The length of cecum ligated, and the gauge of needle used for perforation allows graded response. AvrA will be delivered via the pulmonary route or intravenously as anti-ICAM-1 or anti-ACE-2 coated AvrA-MSA NP, uncoated AvrA-MSA NP and inert MSA NP. All particles will contain 15% AF647 labelled MSA. Animals will be sacrificed, and responses will be measured by serum ELISA for inflammatory cytokines and chemokines, circulating neutrophils, survival, and histological parameters of inflammation in tissues such as lung and heart. Tissue sections will also be evaluated by microscopy for fluorescence.

4.2.1.1 Diabetes

Diabetes affects over 400 million people around the world and is the 7th leading cause of death in the United States[124], [125] 90 percent of reported cases of diabetes are Type 2[124]. In Type 2 diabetes, the body does not respond normally to insulin, and develops high blood sugar. Insulin is a hormone made by beta(β) cells in the pancreas that lets blood sugar into cells. If cells do not take up the sugar, the pancreas makes more insulin until the cells stop responding and sugar accumulates in the blood. Type 2 diabetes develops over time; however, a poor diet, lack of physical activity, genetics, and obesity are risk factors. As a future project, protein nanoparticles would be engineered to deliver therapeutic proteins intracellularly to β-cells of the pancreas and demonstrate the functionality by delivery of AvrA, an effector protein from *Salmonella*, to inhibit inflammation that results in β-cell death and a progressive loss of insulin production found in pre-diabetes and Type 2 diabetes. Ultimately, NP drug delivery to β-cells in the pancreas is a novel concept that has yet to be examined.

4.2.1.2 Inhibiting Beta Death

Recently, Type 2 diabetes has been confirmed as an inflammatory disease; however, there is little information regarding whether anti-inflammatory therapies might be beneficial. The transcription of NF- κB in obese people increases the risk for Type 2 diabetes and up regulates transcription of pro-inflammatory cytokines like IL-6, IL1 α and TNF-α[126], JNK has been widely investigated in obesity models of insulin resistance and shown to drive insulin resistance in obesity[127]. Activation of the JNK pathway has been linked to the inflammatory response and oxidative stress in diabetic pathophysiology[128]. One significant challenge with AvrA is delivering the enzyme into cells, as its large size prevents diffusion through cell membranes.

However, our lab previously incorporated AvrA into albumin protein NPs and successfully delivered it locally to the gastrointestinal tract to treat inflammatory bowel disease (IBD) in mice[37]. The AvrA nanoparticles were not targeted to specific cells within the gut. The challenge for this project is specifically targeting pancreatic β-cells. However, pancreatic islets where β-cells reside are highly vascularized. anti-ICAM1 or anti-ACE2 coated NPs could allow intracellular delivery to these cells. Targeted protein NPs can be utilized to create a novel therapeutic delivery method that will block inflammation and prevent β-cell death**.**

4.2.1.3 Engineering Protein Nanoparticles

Protein NPs are fabricated by adding a desolvant, acetone, to an aqueous protein solution. The subsequent addition of a cleavable water-soluble, amine-reactive, reducible crosslinker ensures protein stability until endocytosis. Mixtures of AvrA and bovine serum albumin (BSA) will be integrated into NPs to control NP size and preserve AvrA bioactivity. The BSA- AvrA nanoparticles will be coated with exendin-4 and crosslinked to stabilize (Figure 4.1). Exendin-4 is a GLP-1 (glucagon-like peptide-1) analogue that targets GLP-1 receptor, a β-cell biomarker that is highly expressed[129] an alternative to GLP-1R, G protein-coupled receptor (GPR44), a receptor for prostaglandin D2 (PGD2) and DiGeorge syndrome critical region gene 2 (DGCR2), an adhesion receptor, are both β cell specific proteins that are highly expressed. Their antibodies, anti- PGD2 and anti-DGCR2, will serve as targeting ligands on the surface of the engineered NPs using the same method of coating for exendin- 4[130]. The physiochemical properties of BSA-Avra-exendin-4 nanoparticles will be characterized by SDS- PAGE to confirm the coating and Dynamic Light Scattering to confirm NP size.

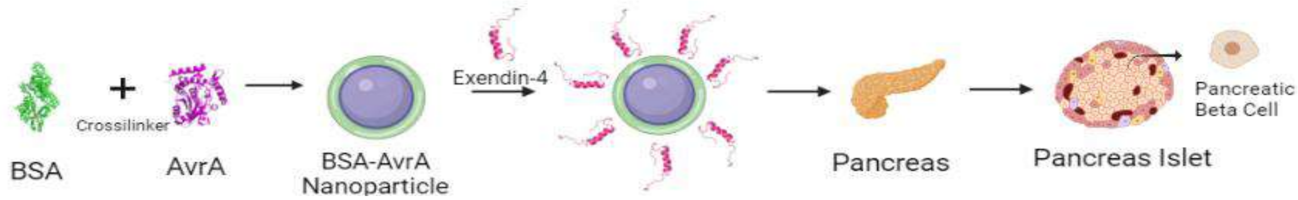

Figure 4.1 Schematic of BSA-AvrA NP coated with Exendin-4 targeting the pancreatic Beta Cell

4.2.1.4 EndoC-BH1 Nanoparticle Interaction

To determine uptake, EndoC- βH1 cells will be treated with fluorescently labeled BSA-AvrA-exendin-4/anti-PGD2/anti-DGCR2 or BSA-AvrA NPs at 2 or 5 µg/ml albumin concentration. After 24 hrs., the cells will be examined with flow cytometry. Confocal Microscopy will be used to confirm cellular uptake of the NPs. To determine the functionality of AvrA treatment, the β-cells will be stimulated with TNF- α and a cell stress assay will be used to determine when the cells endure endoplasmic reticulum (ER) stress, which induces β-cell dysfunction[131] addition, the cytokines secreted will be quantified by ELISA. EndoC- βH1 cells will be lysed and analyzed in the Human Insulin Kit to determine insulin secretion. The Cell Titer-Glo 2.0 Assay will be used to quantify the amount of ATP present, which indicates metabolically active cells[132]. If this *in vitro* work is successful, the next steps would be to assess these particles in a murine study.

APPENDIX A. IVIS IMAGING

A.1 2hr IVIS Images

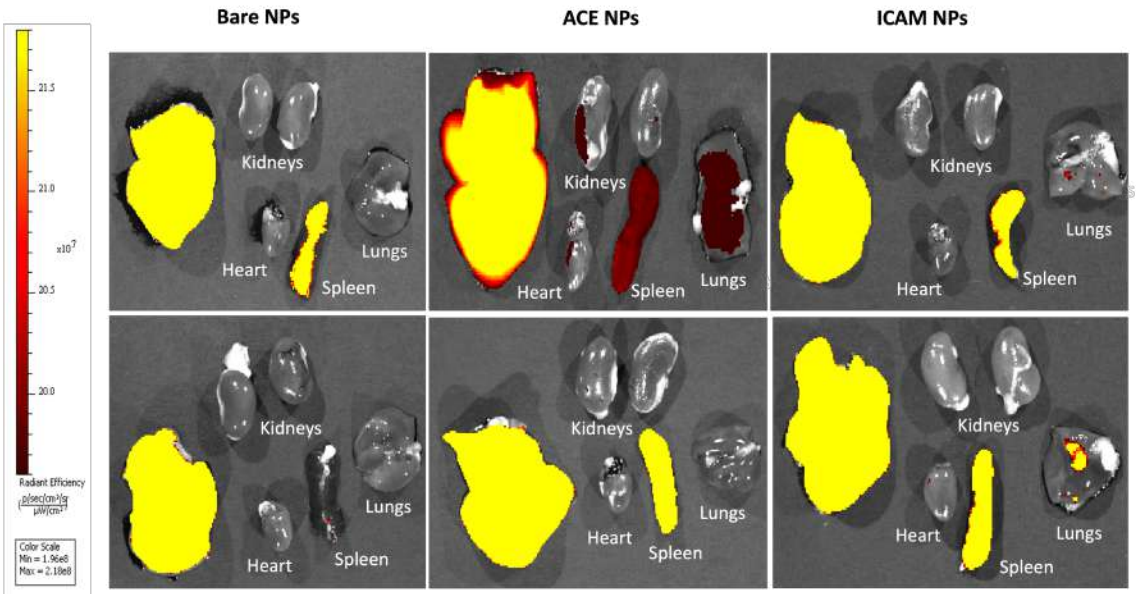

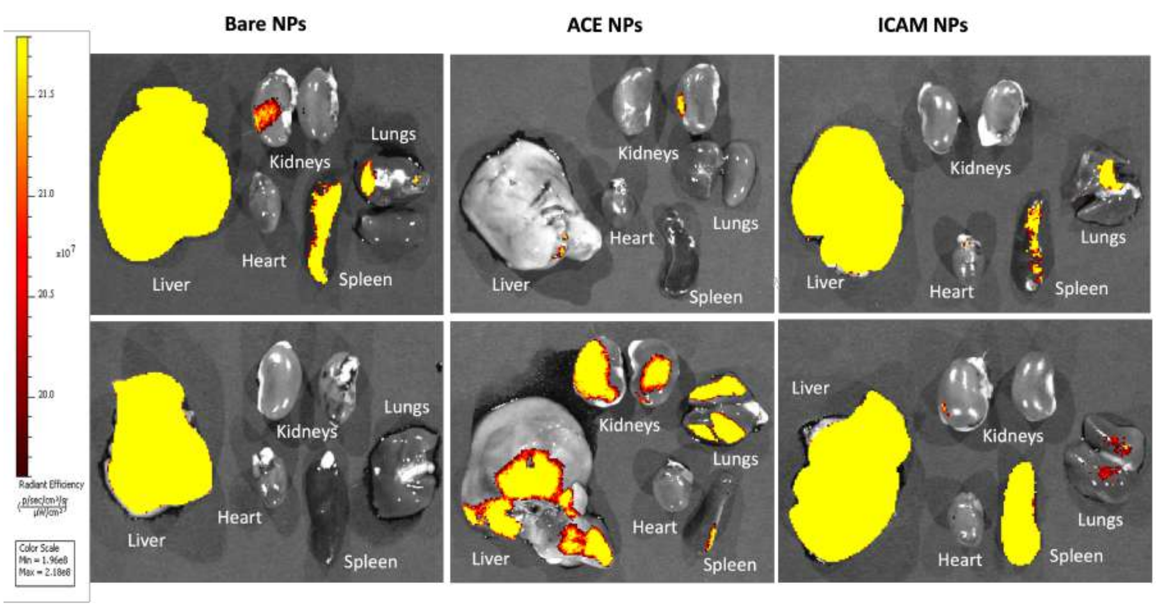

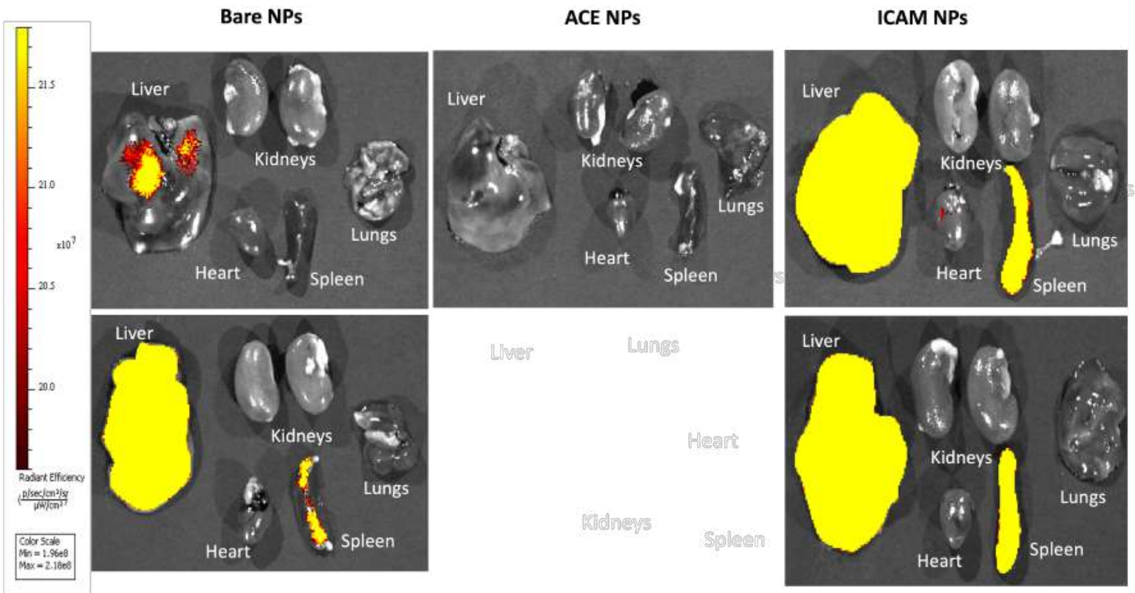

A.2 6hr IVIS Images

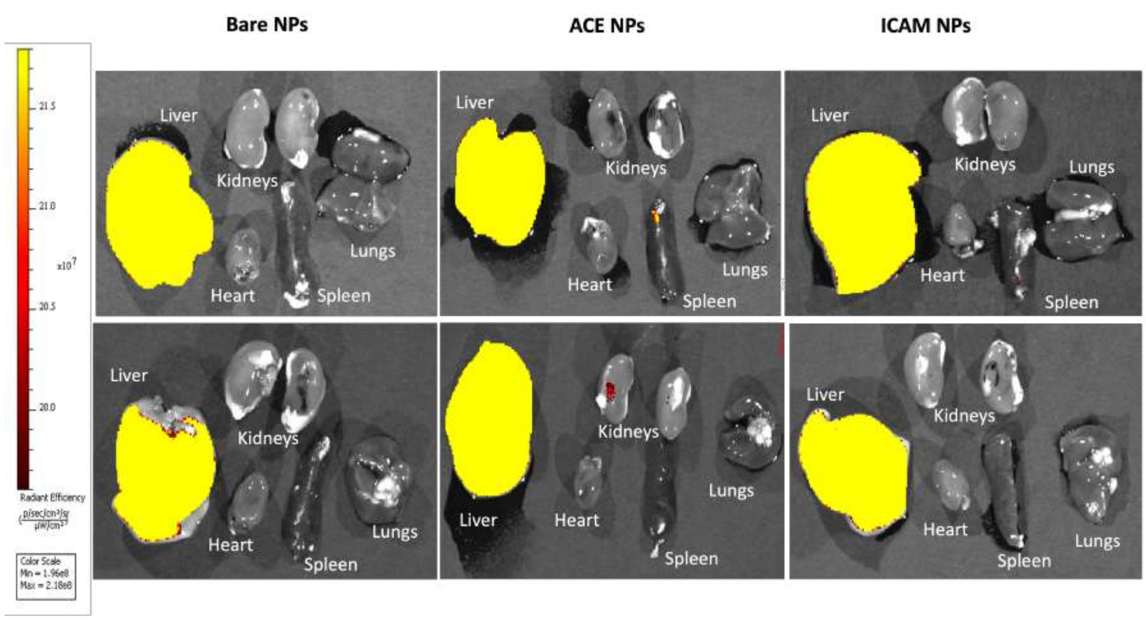

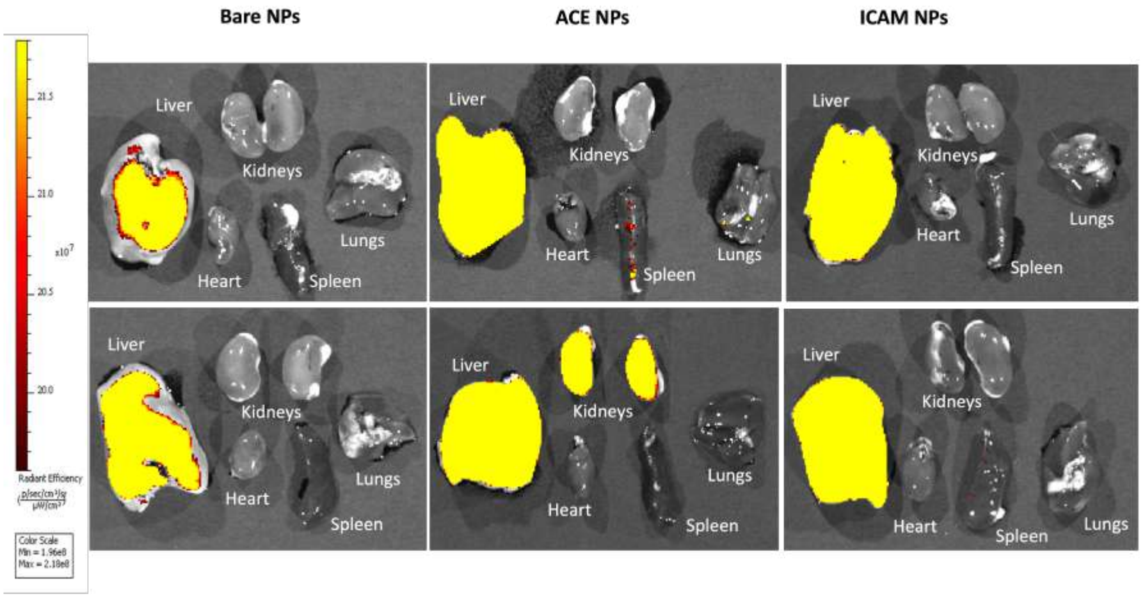
Bare NPs
ACE NPs
ICAM NPs
21.5
21.0
20.5
20.0
x10^7
Radiant Efficiency
Color Scale
Min = 1.96e8
Max = 2.18e8
Liver
Kidneys
Heart
Spleen
Lungs

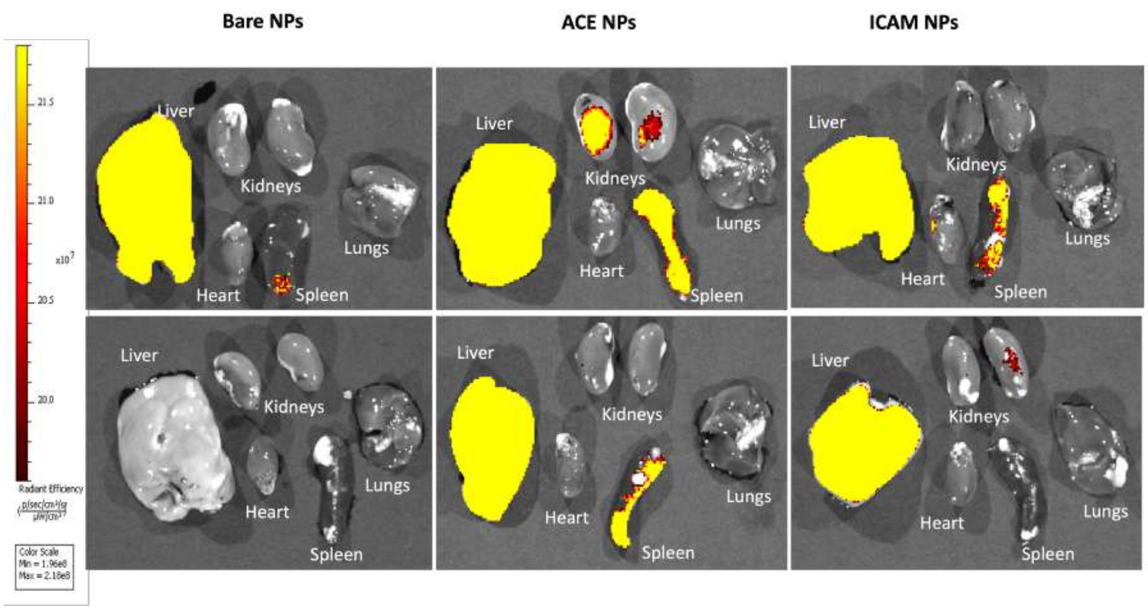
Bare NPs
ACE NPs
ICAM NPs
21.5
21.0
20.5
20.0
x10^7
Radiant Efficiency
Color Scale
Min = 1.96e8
Max = 2.18e8
Liver
Kidneys
Heart
Spleen
Lungs

A.3 24hr IVIS Images

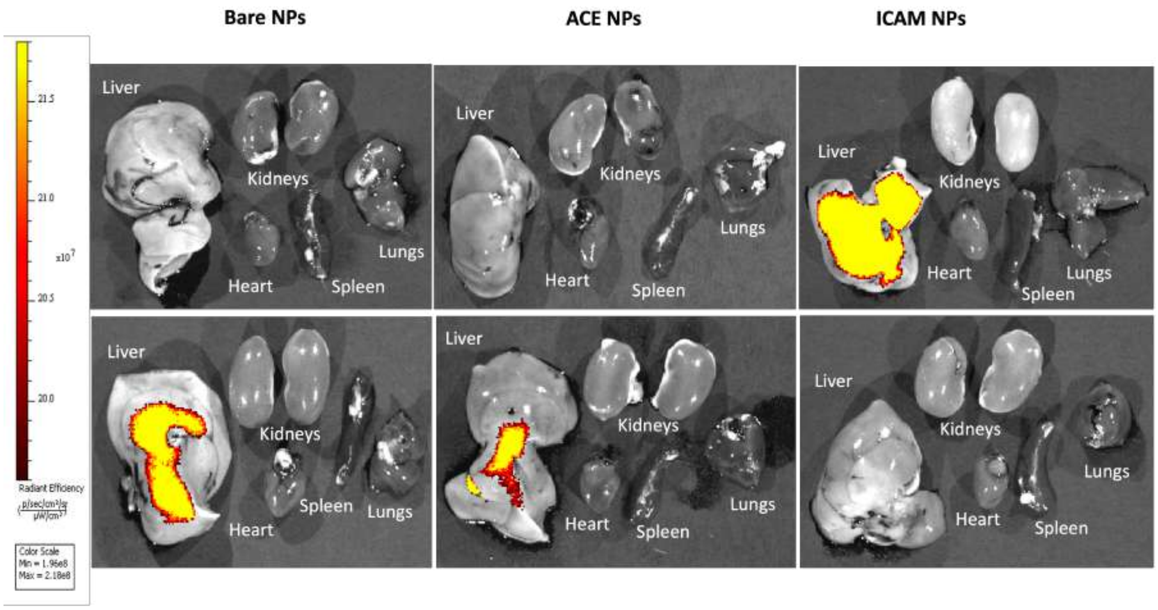

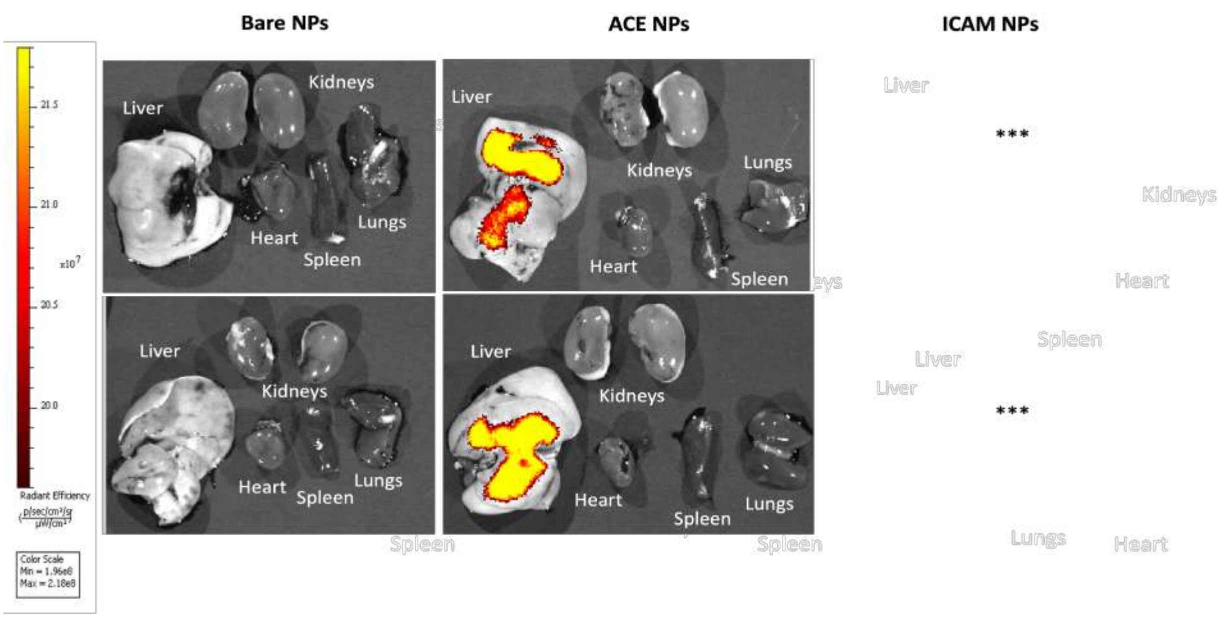

(*** Signify mice that passed away before imaging***)

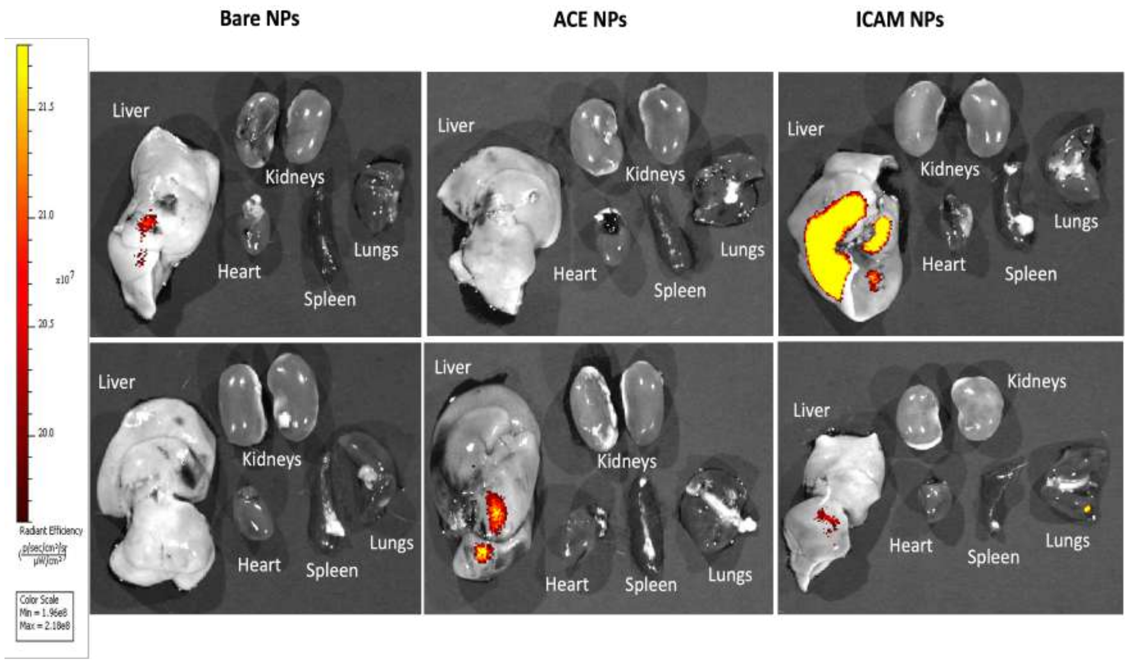
Bare NPs
ACE NPs
ICAM NPs
Liver
Kidneys
Heart
Spleen
Lungs
Radiant Efficiency
Color Scale
Min = 1.96e8
Max = 2.18e8

REFERENCES

[1] R. Pahwa, A. Goyal, P. Bansal, and I. Jialal, "Chronic Inflammation Continuing Education Activity." Accessed: Jul. 14, 2022. [Online]. Available: https://pubmed.ncbi.nlm.nih.gov/29630225/

[2] D. Furman *et al.*, "Chronic inflammation in the etiology of disease across the life span," *Nature Medicine*, vol. 25, no. 12, pp. 1822–1832, Dec. 2019, doi: 10.1038/s41591-019-0675-0.

[3] M. E. Kotas and R. Medzhitov, "Homeostasis, Inflammation, and Disease Susceptibility," *Cell*, vol. 160, no. 5, p. 816, Feb. 2015, doi: 10.1016/J.CELL.2015.02.010.

[4] R. Ginwala, R. Bhavsar, D. I. Gaulle Chigbu, P. Jain, and Z. K. Khan, "Potential Role of Flavonoids in Treating Chronic Inflammatory Diseases with a Special Focus on the Anti-Inflammatory Activity of Apigenin," 2019, doi: 10.3390/antiox8020035.

[5] A. G. I. Mainous, B. J. Rooks, and F. A. Orlando, "The Impact of Initial COVID-19 Episode Inflammation Among Adults on Mortality Within 12 Months Post-hospital Discharge," *Frontiers in Medicine*, vol. 0, p. 1241, May 2022, doi: 10.3389/FMED.2022.891375.

[6] R. S. Y. Wong, "Inflammation in COVID-19: from pathogenesis to treatment," *International Journal of Clinical and Experimental Pathology*, vol. 14, no. 7, p. 831, 2021, Accessed: Jun. 26, 2022. [Online]. Available: /pmc/articles/PMC8339720/

[7] H. Wu, R. M. Jones, and A. S. Neish, "The Salmonella effector AvrA mediates bacterial intracellular survival during infection in vivo," *Cell Microbiol*, vol. 14, no. 1, pp. 28–39, Jan. 2012, doi: 10.1111/J.1462-5822.2011.01694.X.

[8] K. Ling, H. Wu, A. S. Neish, and J. A. Champion, "Alginate/chitosan microparticles for gastric passage and intestinal release of therapeutic protein nanoparticles," *Journal of Controlled Release*, vol. 295, pp. 174–186, Feb. 2019, doi: 10.1016/J.JCONREL.2018.12.017.

[9] S. Senapati, A. K. Mahanta, S. Kumar, and P. Maiti, "Controlled drug delivery vehicles for cancer treatment and their performance," *Signal Transduction and Targeted Therapy*, vol. 3, no. 1, Dec. 2018, doi: 10.1038/S41392-017-0004-3.

[10] A. A. Yetisgin, S. Cetinel, M. Zuvin, A. Kosar, and O. Kutlu, "Therapeutic Nanoparticles and Their Targeted Delivery Applications," *Molecules*, vol. 25, no. 9, May 2020, doi: 10.3390/MOLECULES25092193.

[11] Y. Yao *et al.*, "Nanoparticle-Based Drug Delivery in Cancer Therapy and Its Role in Overcoming Drug Resistance," *Frontiers in Molecular Biosciences*, vol. 7, p. 193, Aug. 2020, doi: 10.3389/FMOLB.2020.00193/BIBTEX.

[12] M. R. Antognazza, L. Latterini, F. Cellesi, M. I. Martinez Espinoza, F. Moncalvo, and M. Isabel Martinez Espinoza, “Nanosized Delivery Systems for Therapeutic Proteins: Clinically Validated Technologies and Advanced Development Strategies,” 2020, doi: 10.3389/fbioe.2020.00089.

[13] W. B. Geho, H. C. Geho, J. R. Lau, and T. J. Gana, “Hepatic-Directed Vesicle Insulin: A Review of Formulation Development and Preclinical Evaluation,” 2009. [Online]. Available: www.journalofdst.org

[14] S. Kube *et al.*, “Fusogenic Liposomes as Nanocarriers for the Delivery of Intracellular Proteins,” 2017, doi: 10.1021/acs.langmuir.6b04304.

[15] S. Xie *et al.*, “Enhanced intracellular delivery and antibacterial efficacy of enrofloxacin-loaded docosanoic acid solid lipid nanoparticles against intracellular Salmonella,” *Scientific Reports 2017 7:1*, vol. 7, no. 1, pp. 1–9, Jan. 2017, doi: 10.1038/srep41104.

[16] P. Ghasemiyeh and S. Mohammadi-Samani, “Solid lipid nanoparticles and nanostructured lipid carriers as novel drug delivery systems: applications, advantages and disadvantages,” *Research in Pharmaceutical Sciences*, vol. 13, no. 4, p. 288, Aug. 2018, doi: 10.4103/1735-5362.235156.

[17] W. Cui *et al.*, “Article 489 (2020) Application of the Nano-Drug Delivery System in Treatment of Cardiovascular Diseases,” *Frontiers in Bioengineering and Biotechnology | www.frontiersin.org*, vol. 1, p. 489, 2020, doi: 10.3389/fbioe.2019.00489.

[18] A. Gagliardi *et al.*, “Biodegradable Polymeric Nanoparticles for Drug Delivery to Solid Tumors”, doi: 10.3389/fphar.2021.601626.

[19] D. Wei *et al.*, “Soybean Lecithin-Mediated Nanoporous PLGA Microspheres with Highly Entrapped and Controlled Released BMP-2 as a Stem Cell Platform,” *Small*, vol. 14, no. 22, May 2018, doi: 10.1002/SMLL.201800063.

[20] F. Danhier, E. Ansorena, J. M. Silva, R. Coco, A. le Breton, and V. Préat, “PLGA-based nanoparticles: An overview of biomedical applications,” *Journal of Controlled Release*, vol. 161, no. 2, pp. 505–522, Jul. 2012, doi: 10.1016/J.JCONREL.2012.01.043.

[21] M. Yu, J. Wu, J. Shi, and O. C. Farokhzad, “Nanotechnology for protein delivery: Overview and perspectives,” *J Control Release*, vol. 240, pp. 24–37, Oct. 2016, doi: 10.1016/J.JCONREL.2015.10.012.

[22] L. Hasadsri, J. Kreuter, H. Hattori, T. Iwasaki, and J. M. George, “Functional Protein Delivery into Neurons Using Polymeric Nanoparticles *,” *Journal of Biological Chemistry*, vol. 284, no. 11, pp. 6972–6981, Mar. 2009, doi: 10.1074/JBC.M805956200.

[23] T. del Castillo-Santaella *et al.*, “pharmaceutics Formulation, Colloidal Characterization, and In Vitro Biological Effect of BMP-2 Loaded PLGA Nanoparticles for Bone Regeneration”, doi: 10.3390/pharmaceutics11080388.

[24] A. Suriya Prabha, R. Dorothy, S. Jancirani, S. Rajendran, G. Singh, and S. Senthil Kumaran, “Recent advances in the study of toxicity of polymer-based nanomaterials,” *Nanotoxicity: Prevention and Antibacterial Applications of Nanomaterials*, pp. 143–165, Jan. 2020, doi: 10.1016/B978-0-12-819943-5.00007-5.

[25] L. Peltonen, M. Singhal, and J. Hirvonen, “Principles of nanosized drug delivery systems,” *Nanoengineered Biomaterials for Advanced Drug Delivery*, pp. 3–25, Jan. 2020, doi: 10.1016/B978-0-08-102985-5.00001-2.

[26] W. Li *et al.*, “Nanoparticle-Based Drug Delivery in Cancer Therapy and Its Role in Overcoming Drug Resistance,” *Front. Mol. Biosci*, vol. 7, p. 193, 2020, doi: 10.3389/fmolb.2020.00193.

[27] P. Ghosh *et al.*, “Intracellular Delivery of a Membrane-Impermeable Enzyme in Active Form Using Functionalized Gold Nanoparticles”, doi: 10.1021/ja907887z.

[28] K. Lee *et al.*, “Nanoparticle delivery of Cas9 ribonucleoprotein and donor DNA in vivo induces homology-directed DNA repair HHS Public Access,” vol. 1, pp. 889–901, 2017, doi: 10.1038/s41551-017-0137-2.

[29] M. Müllner, A. Schallon, A. Walther, R. Freitag, and A. H. E. Müller, “Clickable, biocompatible, and fluorescent hybrid nanoparticles for intracellular delivery and optical imaging,” *Biomacromolecules*, vol. 11, no. 2, pp. 390–396, Feb. 2010, doi: 10.1021/BM901099P/SUPPL_FILE/BM901099P_SI_001.PDF.

[30] M. H. Ali and B. Imperiali, “Protein oligomerization: how and why,” *Bioorg Med Chem*, vol. 13, no. 17, pp. 5013–5020, Sep. 2005, doi: 10.1016/J.BMC.2005.05.037.

[31] A. Zeltins, “Construction and characterization of virus-like particles: a review,” *Mol Biotechnol*, vol. 53, no. 1, pp. 92–107, Jan. 2013, doi: 10.1007/S12033-012-9598-4.

[32] S. J. Kaczmarczyk, K. Sitaraman, H. A. Young, S. H. Hughes, and D. K. Chatterjee, “Protein delivery using engineered virus-like particles”, doi: 10.1073/pnas.1101874108.

[33] C. Voelkel *et al.*, “Protein transduction from retroviral Gag precursors,” *Proc Natl Acad Sci U S A*, vol. 107, no. 17, p. 7805, Apr. 2010, doi: 10.1073/PNAS.0914517107.

[34] T. Z. Chang and J. A. Champion, “Protein and Peptide Nanocluster Vaccines,” *Curr Top Microbiol Immunol*, vol. 433, pp. 107–130, 2021, doi: 10.1007/82_2020_228.

[35] C. Weber, C. Coester, J. Kreuter, and K. Langer, “Desolvation process and surface characterisation of protein nanoparticles,” *Int J Pharm*, vol. 194, no. 1, pp. 91–102, Jan. 2000, doi: 10.1016/S0378-5173(99)00370-1.

[36] L. P. Herrera Estrada and J. A. Champion, “Protein nanoparticles for therapeutic protein delivery,” *Biomater Sci*, vol. 3, no. 6, pp. 787–799, Jun. 2015, doi: 10.1039/C5BM00052A.

[37] L. Herrera Estrada *et al.*, “Bioengineering Bacterially Derived Immunomodulants: A Therapeutic Approach to Inflammatory Bowel Disease,” 2017, doi: 10.1021/acsnano.7b03239.

[38] V. Sanna and M. Sechi, “Therapeutic Potential of Targeted Nanoparticles and Perspective on Nanotherapies,” *Cite This: ACS Med. Chem. Lett*, vol. 11, pp. 1069–1073, 2020, doi: 10.1021/acsmedchemlett.0c00075.

[39] A. D. Friedman, S. E. Claypool, and R. Liu, “The Smart Targeting of Nanoparticles,” *Curr Pharm Des*, vol. 19, no. 35, p. 6315, Apr. 2013, doi: 10.2174/13816128113199990375.

[40] S. Muro, X. Cui, C. Gajewski, J.-C. Murciano, V. R. Muzykantov, and M. Koval, “Slow intracellular trafficking of catalase nanoparticles targeted to ICAM-1 protects endothelial cells from oxidative stress,” *American Journal of Physiology-Cell Physiology*, 2003, doi: 10.1152/ajpcell.00099.2003.

[41] M. Howard, B. J. Zern, A. C. Anselmo, V. v. Shuvaev, S. Mitragotri, and V. Muzykantov, “Vascular targeting of nanocarriers: Perplexing aspects of the seemingly straightforward paradigm,” *ACS Nano*, vol. 8, no. 5, pp. 4100–4132, May 2014, doi: 10.1021/NN500136Z/ASSET/IMAGES/LARGE/NN-2014-00136Z_0015.JPEG.

[42] V. v. Shuvaev, J. S. Brenner, and V. R. Muzykantov, “Targeted endothelial nanomedicine for common acute pathological conditions,” *Journal of Controlled Release*, vol. 219, pp. 576–595, Dec. 2015, doi: 10.1016/J.JCONREL.2015.09.055.

[43] C. Y. Zhang *et al.*, “PH-Responsive Nanoparticles Targeted to Lungs for Improved Therapy of Acute Lung Inflammation/Injury,” *ACS Applied Materials and Interfaces*, vol. 11, no. 18, pp. 16380–16390, May 2019, doi: 10.1021/ACSAMI.9B04051/ASSET/IMAGES/LARGE/AM-2019-04051M_0005.JPEG.

[44] “Multifunctional Inorganic Nanoparticles for Imaging, Targeting, and Drug Delivery”.

[45] Samira Guccione, King C P Li, and Mark D Bednarski, “Vascular-targeted nanoparticles for molecular imaging and therapy ,” *Methods in Enzymology*, vol. 386, pp. 219–236, 2004.

[46] E. Amstad, S. Zurcher, A. Mashaghi, J. Y. Wong, M. Textor, and E. Reimhult, "Surface functionalization of single superparamagnetic iron oxide nanoparticles for targeted Magnetic resonance imaging," *Small*, vol. 5, no. 11, pp. 1334–1342, Jun. 2009, doi: 10.1002/SMLL.200801328.

[47] A.-L. Bailly *et al.*, "In vivo evaluation of safety, biodistribution and pharmacokinetics of laser-synthesized gold nanoparticles", doi: 10.1038/s41598-019-48748-3.

[48] C. C. Fleischer and C. K. Payne, "Secondary structure of corona proteins determines the cell surface receptors used by nanoparticles," *Journal of Physical Chemistry B*, vol. 118, no. 49, pp. 14017–14026, Dec. 2014, doi: 10.1021/JP502624N/SUPPL_FILE/JP502624N_SI_001.PDF.

[49] A. M. Merlot, D. S. Kalinowski, and D. R. Richardson, "Unraveling the mysteries of serum albumin-more than just a serum protein," *Frontiers in Physiology*, vol. 5 AUG, 2014, doi: 10.3389/fphys.2014.00299.

[50] K. Jin, Z. Luo, B. Zhang, and Z. Pang, "Biomimetic nanoparticles for inflammation targeting," *Acta Pharmaceutica Sinica B*, vol. 8, no. 1. Chinese Academy of Medical Sciences, pp. 23–33, Jan. 01, 2018. doi: 10.1016/j.apsb.2017.12.002.

[51] R. Carlisle, L. W. Seymour, and C. C. Coussios, "Targeting of liposomes via PSGL1 for enhanced tumor accumulation," *Pharmaceutical Research*, vol. 30, no. 2, pp. 352–361, Feb. 2013, doi: 10.1007/s11095-012-0875-5.

[52] M. Voinea, I. Manduteanu, E. Dragomir, M. Capraru, and M. Simionescu, "Immunoliposomes directed toward VCAM-1 interact specifically with activated endothelial cells--a potential tool for specific drug delivery.," *Pharmaceutical Research*, vol. 22, no. 11, pp. 1906–1917, Aug. 2005, doi: 10.1007/S11095-005-7247-3.

[53] P. G. M. Bloemen *et al.*, "Adhesion molecules: a new target for immunoliposome-mediated drug delivery," *FEBS Letters*, vol. 357, no. 2, pp. 140–144, Jan. 1995, doi: 10.1016/0014-5793(94)01350-A.

[54] S. Muro, C. Gajewski, M. Koval, and V. R. Muzykantov, "ICAM-1 recycling in endothelial cells: a novel pathway for sustained intracellular delivery and prolonged effects of drugs," *Blood*, vol. 105, no. 2, pp. 650–658, Jan. 2005, doi: 10.1182/BLOOD-2004-05-1714.

[55] S. Muro and V. Muzykantov, "Targeting of Antioxidant and Anti-Thrombotic Drugs to Endothelial Cell Adhesion Molecules," *Current Pharmaceutical Design*, vol. 11, no. 18, pp. 2383–2401, Jul. 2005, doi: 10.2174/1381612054367274.

[56] S. Muro and V. Muzykantov, "Targeting of antioxidant and anti-thrombotic drugs to endothelial cell adhesion molecules," *Curr Pharm Des*, vol. 11, no. 18, pp. 2383–2401, Jul. 2005, doi: 10.2174/1381612054367274.

[57] D. Scholz *et al.*, "Expression of adhesion molecules is specific and time-dependent in cytokine-stimulated endothelial cells in culture," *Cell and Tissue Research*, vol. 284, no. 3, pp. 415–423, 1996, doi: 10.1007/S004410050602.

[58] G. A. Koning, R. M. Schiffelers, and G. Storm, "Endothelial cells at inflammatory sites as target for therapeutic intervention," *Endothelium: Journal of Endothelial Cell Research*, vol. 9, no. 3, pp. 161–171, 2002, doi: 10.1080/10623320213631.

[59] A. K. Hubbard and R. Rothlein, "Intercellular adhesion molecule-1 (ICAM-1) expression and cell signaling cascades," *Free Radical Biology and Medicine*, vol. 28, no. 9, pp. 1379–1386, May 2000, doi: 10.1016/S0891-5849(00)00223-9.

[60] M. Soy, G. Keser, P. Atagündüz, F. Tabak, I. Atagündüz, and S. Kayhan, "Cytokine storm in COVID-19: pathogenesis and overview of anti-inflammatory agents used in treatment," *Clinical Rheumatology*, vol. 39, no. 7. Springer, pp. 2085–2094, Jul. 01, 2020. doi: 10.1007/s10067-020-05190-5.

[61] Wenhui Li *et al.*, "Angiotensin-converting enzyme 2 is a functional receptor for the SARS coronavirus," *Nature*, pp. 450–454, 2003, doi: https://doi.org/10.1038/nature02145.

[62] I. Hamming, W. Timens, M. L. C. Bulthuis, A. T. Lely, G. J. Navis, and H. van Goor, "Tissue distribution of ACE2 protein, the functional receptor for SARS coronavirus. A first step in understanding SARS pathogenesis," *Journal of Pathology*, vol. 203, no. 2, pp. 631–637, Jun. 2004, doi: 10.1002/path.1570.

[63] D. A. Cronkite and T. M. Strutt, "The regulation of inflammation by innate and adaptive lymphocytes," *Journal of Immunology Research*, vol. 2018, 2018, doi: 10.1155/2018/1467538.

[64] G. di Mauro, C. Scavone, C. Rafaniello, F. Rossi, and A. Capuano, "SARS-Cov-2 infection: Response of human immune system and possible implications for the rapid test and treatment," 2020, doi: 10.1016/j.intimp.2020.106519.

[65] M. Catanzaro, F. Fagiani, M. Racchi, E. Corsini, S. Govoni, and C. Lanni, "Immune response in COVID-19: addressing a pharmacological challenge by targeting pathways triggered by SARS-CoV-2," *Signal Transduction and Targeted Therapy*, vol. 5, no. 1. Springer Nature, Dec. 01, 2020. doi: 10.1038/s41392-020-0191-1.

[66] C. D. Russell, J. E. Millar, and J. K. Baillie, "Clinical evidence does not support corticosteroid treatment for 2019-nCoV lung injury," *Lancet*, vol. 395, no. 10223, pp. 473–475, Feb. 2020, doi: 10.1016/S0140-6736(20)30317-2.

[67] J. H. Beigel *et al.*, "Remdesivir for the Treatment of Covid-19 — Final Report," *New England Journal of Medicine*, vol. 383, no. 19, pp. 1813–1826, Nov. 2020, doi: 10.1056/nejmoa2007764.

[68] RECOVERY Collaborative Group *et al.*, "Dexamethasone in Hospitalized Patients with Covid-19," *New England Journal of Medicine*, vol. 384, no. 8, pp. 693–704, Feb. 2021, doi: 10.1056/NEJMoa2021436.

[69] A. Jahanban-Esfahlan, S. Dastmalchi, and S. Davaran, "A simple improved desolvation method for the rapid preparation of albumin nanoparticles," *International Journal of Biological Macromolecules*, vol. 91, pp. 703–709, Oct. 2016, doi: 10.1016/J.IJBIOMAC.2016.05.032.

[70] X. Duan and Y. Li, "Physicochemical Characteristics of Nanoparticles Affect Circulation, Biodistribution, Cellular Internalization, and Traffi cking," 2013, doi: 10.1002/smll.201201390.

[71] S. A. Kulkarni and S.-S. Feng, "Effects of Particle Size and Surface Modification on Cellular Uptake and Biodistribution of Polymeric Nanoparticles for Drug Delivery", doi: 10.1007/s11095-012-0958-3.

[72] S. Pustulka, "Engineering Biomaterial-Protein corona Interactions to mediate biological responses," Georgia Institute of Technology, Atlanta, 2021.

[73] A. Datta-Mannan, J. Lu, D. R. Witcher, D. Leung, Y. Tang, and V. J. Wroblewski, "The interplay of non-specific binding, target-mediated clearance and FcRn interactions on the pharmacokinetics of humanized antibodies," *MAbs*, vol. 7, no. 6, p. 1084, 2015, doi: 10.1080/19420862.2015.1075109.

[74] C. Jobin, C. Hellerbrand, L. L. Licato, D. A. Brenner, and R. B. Sartor, "Mediation by NF-B of cytokine induced expression of intercellular adhesion molecule 1 (ICAM-1) in an intestinal epithelial cell line, a process blocked by proteasome inhibitors", doi: 10.1136/gut.42.6.779.

[75] T. Couffinhal *et al.*, "Tumor Necrosis Factor-o? Stimulates ICAM-1 Expression in Human Vascular Smooth Muscle Cells." [Online]. Available: http://ahajournals.org

[76] P. Thichanpiang, S. Harper, K. Wongprasert, and D. Bates, "TNF-α-induced ICAM-1 expression and monocyte adhesion in human RPE cells is mediated in part through autocrine VEGF stimulation," pp. 781–789, 2014.

[77] L. Cao, C.-S. Li, Z.-X. Liang, and L.-A. Chen, "The effects of perfluorocarbon on ICAM-1 expression in LPS-induced A549 cells and the potential mechanism," Mar. 2016.

[78] E. Folzer *et al.*, "Determination of the Density of Protein Particles Using a Suspended Microchannel Resonator," *Journal of Pharmaceutical Sciences*, vol. 104, no. 12, pp. 4034–4040, Dec. 2015, doi: 10.1002/JPS.24635.

[79] L. A. Cantarero, J. E. Butler, and J. W. Osborne, "The adsorptive characteristics of proteins for polystyrene and their significance in solid-phase imunoassays," *Anal Biochem*, vol. 105, no. 2, pp. 375–382, 1980, doi: 10.1016/0003-2697(80)90473-X.

[80] S. Muro *et al.*, "A novel endocytic pathway induced by clustering endothelial ICAM-1 or PECAM-1," *J Cell Sci*, vol. 116, no. Pt 8, pp. 1599–1609, Apr. 2003, doi: 10.1242/JCS.00367.

[81] I. W. Y. Mak, N. Evaniew, and M. Ghert, "Lost in translation: animal models and clinical trials in cancer treatment," *American Journal of Translational Research*, vol. 6, no. 2, p. 114, 2014, Accessed: Jun. 27, 2022. [Online]. Available: /pmc/articles/PMC3902221/

[82] J. Hsu, T. Bhowmick, S. R. Burks, J. P. Y. Kao, and S. Muro, "Enhancing Biodistribution of Therapeutic Enzymes In Vivo by Modulating Surface Coating and Concentration of ICAM-1-Targeted Nanocarriers," *J Biomed Nanotechnol*, vol. 10, no. 2, p. 345, Feb. 2014, doi: 10.1166/JBN.2014.1718.

[83] R. Ghaffarian, T. Bhowmick, and S. Muro, "Transport of nanocarriers across gastrointestinal epithelial cells by a new transcellular route induced by targeting ICAM-1," *Journal of Controlled Release*, vol. 163, no. 1, pp. 25–33, Oct. 2012, doi: 10.1016/J.JCONREL.2012.06.007.

[84] C. Garnacho *et al.*, "Delivery of Acid Sphingomyelinase in Normal and Niemann-Pick Disease Mice Using Intercellular Adhesion Molecule-1-Targeted Polymer Nanocarriers," *Journal of Pharmacology and Experimental Therapeutics*, vol. 325, no. 2, pp. 400–408, May 2008, doi: 10.1124/JPET.107.133298.

[85] D. van Haute and J. M. Berlin, "Therapeutic Delivery Perspective Challenges in realizing selectivity for nanoparticle biodistribution and clearance: lessons from gold nanoparticles," *Ther. Deliv*, vol. 8, no. 9, pp. 763–774, 2017, doi: 10.4155/tde-2017-0057.

[86] Q. Lin, P. Fathi, and X. Chen, "Nanoparticle delivery in vivo: A fresh look from intravital imaging," *EBioMedicine*, vol. 59, Sep. 2020, doi: 10.1016/J.EBIOM.2020.102958.

[87] A. Boey and H. K. Ho, "All Roads Lead to the Liver: Metal Nanoparticles and Their Implications for Liver Health," *Small*, vol. 16, no. 21, p. 2000153, May 2020, doi: 10.1002/SMLL.202000153.

[88] A. C. Anselmo *et al.*, "Delivering nanoparticles to lungs while avoiding liver and spleen through adsorption on red blood cells," *ACS Nano*, vol. 7, no. 12, pp. 11129–11137, Dec. 2013, doi: 10.1021/NN404853Z/SUPPL_FILE/NN404853Z_SI_001.PDF.

[89] Y. N. Zhang, W. Poon, A. J. Tavares, I. D. McGilvray, and W. C. W. Chan, "Nanoparticle–liver interactions: Cellular uptake and hepatobiliary elimination," *Journal of Controlled Release*, vol. 240, pp. 332–348, Oct. 2016, doi: 10.1016/J.JCONREL.2016.01.020.

[90] M. Longmire, P. L. Choyke, and H. Kobayashi, "Clearance Properties of Nano-sized Particles and Molecules as Imaging Agents: Considerations and Caveats," *Nanomedicine (Lond)*, vol. 3, no. 5, p. 703, Oct. 2008, doi: 10.2217/17435889.3.5.703.

[91] M. Cataldi, C. Vigliotti, T. Mosca, M. R. Cammarota, and D. Capone, "Emerging Role of the Spleen in the Pharmacokinetics of Monoclonal Antibodies, Nanoparticles and Exosomes," *International Journal of Molecular Sciences*, vol. 18, no. 6, Jun. 2017, doi: 10.3390/IJMS18061249.

[92] L. Arms *et al.*, "Advantages and limitations of current techniques for analyzing the biodistribution of nanoparticles," *Frontiers in Pharmacology*, vol. 9, no. AUG, p. 802, Aug. 2018, doi: 10.3389/FPHAR.2018.00802/BIBTEX.

[93] S. Hua, P. C.-P. physician, and undefined 2013, "Targeted nanoparticles that mimic immune cells in pain control inducing analgesic and anti-inflammatory actions: a potential novel treatment of acute and," *painphysicianjournal.com*, Accessed: Jun. 29, 2022. [Online]. Available: https://www.painphysicianjournal.com/current/pdf?article=MTkxNQ%3D%3D&journal=75

[94] R. Kumar *et al.*, "In vivo Biodistribution and Clearance Studies using Multimodal ORMOSIL Nanoparticles," *ACS Nano*, vol. 4, no. 2, p. 699, Feb. 2010, doi: 10.1021/NN901146Y.

[95] J. Kim *et al.*, "Use of nanoparticle contrast agents for cell tracking with computed tomography," *ACS Publications*, vol. 28, no. 6, pp. 1581–1597, Jun. 2017, doi: 10.1021/acs.bioconjchem.7b00194.

[96] V. Koo, … P. H.-A. C., and undefined 2006, "Non-invasive in vivo imaging in small animal research," *content.iospress.com*, vol. 28, pp. 127–139, 2006, Accessed: Jun. 29, 2022. [Online]. Available: https://content.iospress.com/articles/analytical-cellular-pathology/clo348

[97] J. Wolfram *et al.*, "The nano-plasma interface: implications of the protein corona," *Colloids Surf B Biointerfaces*, vol. 0, p. 17, Dec. 2014, doi: 10.1016/J.COLSURFB.2014.02.035.

[98] K. Nagasawa *et al.*, "Possible involvement of gap junctions in the barrier function of tight junctions of brain and lung endothelial cells," *Journal of Cellular Physiology*, vol. 208, no. 1, pp. 123–132, Jul. 2006, doi: 10.1002/JCP.20647.

[99] M. L. Fehrenbach, G. Cao, J. T. Williams, J. M. Finklestein, and H. M. DeLisser, "Isolation of murine lung endothelial cells," *American Journal of Physiology - Lung Cellular and Molecular Physiology*, vol. 296, no. 6, pp. 1096–1103, Jun. 2009, doi: 10.1152/AJPLUNG.90613.2008/ASSET/IMAGES/LARGE/ZH50060954310006.JPEG.

[100] S. Gebb and T. Stevens, "On lung endothelial cell heterogeneity," *Microvascular Research*, vol. 68, no. 1, pp. 1–12, Jul. 2004, doi: 10.1016/J.MVR.2004.02.002.

[101] P. Malyala and M. Singh, "Endotoxin Limits in Formulations for Preclinical Research," *Journal of Pharmaceutical Sciences*, vol. 97, no. 6, pp. 2041–2044, Jun. 2008, doi: 10.1002/JPS.21152.

[102] M. Tarhini, I. Benlyamani, S. Hamdani, G. Agusti, and H. Fessi, "Protein-Based Nanoparticle Preparation via Nanoprecipitation Method," Mar. 2018.

[103] M. Y. Li, L. Li, Y. Zhang, and X. S. Wang, "Expression of the SARS-CoV-2 cell receptor gene ACE2 in a wide variety of human tissues," *Infectious Diseases of Poverty*, vol. 9, no. 1, pp. 1–7, Apr. 2020, doi: 10.1186/S40249-020-00662-X/FIGURES/2.

[104] C. Tsioutis *et al.*, "Body Localization of ACE-2: On the Trail of the Keyhole of SARS-CoV-2," *Frontiers in Medicine | www.frontiersin.org*, vol. 7, p. 594495, 2020, doi: 10.3389/fmed.2020.594495.

[105] I. v. Zelepukin *et al.*, "Fast processes of nanoparticle blood clearance: Comprehensive study," *Journal of Controlled Release*, vol. 326, pp. 181–191, Oct. 2020, doi: 10.1016/J.JCONREL.2020.07.014.

[106] F. Alexis, E. Pridgen, L. K. Molnar, and O. C. Farokhzad, "Factors affecting the clearance and biodistribution of polymeric nanoparticles," *Molecular Pharmaceutics*, vol. 5, no. 4, pp. 505–515, Jul. 2008, doi: 10.1021/MP800051M/ASSET/IMAGES/LARGE/MP-2008-00051M_0001.JPEG.

[107] R. Rossin, S. Muro, M. J. Welch, V. R. Muzykantov, and D. P. Schuster, "In Vivo Imaging of 64 Cu-Labeled Polymer Nanoparticles Targeted to the Lung Endothelium," *J Nucl Med*, vol. 49, pp. 103–111, 2008, doi: 10.2967/jnumed.107.045302.

[108] M. Hadjidemetriou and K. Kostarelos, "Nanomedicine: Evolution of the nanoparticle corona," *Nat Nanotechnol*, vol. 12, no. 4, pp. 288–290, May 2017, doi: 10.1038/NNANO.2017.61.

[109] P. C. Ke, S. Lin, W. J. Parak, T. P. Davis, and F. Caruso, "A Decade of the Protein Corona," *ACS Nano*, vol. 11, no. 12, pp. 11773–11776, Dec. 2017, doi: 10.1021/ACSNANO.7B08008.

[110] M. Lundqvist, J. Stigler, G. Elia, I. Lynch, T. Cedervall, and K. A. Dawson, "Nanoparticle size and surface properties determine the protein corona with possible implications for biological impacts," *Proc Natl Acad Sci U S A*, vol. 105, no. 38, pp. 14265–14270, Sep. 2008, doi: 10.1073/PNAS.0805135105/SUPPL_FILE/ST1.XLS.

[111] T. Cedervall *et al.*, "Understanding the nanoparticle-protein corona using methods to quantify exchange rates and affinities of proteins for nanoparticles," *Proc Natl Acad*

Sci U S A, vol. 104, no. 7, pp. 2050–2055, Feb. 2007, doi: 10.1073/PNAS.0608582104.

[112] I. L. Gunsolus, M. P. S. Mousavi, K. Hussein, P. Bühlmann, and C. L. Haynes, “Effects of Humic and Fulvic Acids on Silver Nanoparticle Stability, Dissolution, and Toxicity,” *Environ Sci Technol*, vol. 49, no. 13, pp. 8078–8086, Jul. 2015, doi: 10.1021/ACS.EST.5B01496.

[113] Y. Zhang, Y. Chen, P. Westerhoff, and J. Crittenden, “Impact of natural organic matter and divalent cations on the stability of aqueous nanoparticles,” *Water Res*, vol. 43, no. 17, pp. 4249–4257, 2009, doi: 10.1016/J.WATRES.2009.06.005.

[114] A. Piloni, C. K. Wong, F. Chen, M. Lord, A. Walther, and M. H. Stenzel, “Surface roughness influences the protein corona formation of glycosylated nanoparticles and alter their cellular uptake,” *Nanoscale*, vol. 11, no. 48, pp. 23259–23267, Dec. 2019, doi: 10.1039/C9NR06835J.

[115] T. Ding and J. Sun, “Formation of Protein Corona on Nanoparticle Affects Different Complement Activation Pathways Mediated by C1q,” *Pharm Res*, vol. 37, no. 1, Jan. 2019, doi: 10.1007/S11095-019-2747-8.

[116] S. Azarmi, W. Roa, and R. Löbenberg, “Targeted delivery of nanoparticles for the treatment of lung diseases,” Feb. 2008.

[117] D. Chenthamara *et al.*, “Therapeutic efficacy of nanoparticles and routes of administration”, doi: 10.1186/s40824-019-0166-x.

[118] E. Leticia, R. Wilson, F. Warren, and L. Raimar, “Effervescent dry powder for respiratory drug delivery,” Mar. 2007.

[119] P. Jani, G. Halbert, and J. Langridge, “Nanoparticle Uptake by the Rat Gastrointestinal Mucosa: Quantitation and Particle Size Dependency Get access Arrow,” Apr. 2011.

[120] K. Marulanda *et al.*, “Intravenous Delivery of Lung-Targeted Nanofibers for Pulmonary Hypertension in Mice,” *Advanced Healthcare Materials*, vol. 10, no. 13, p. 2100302, Jul. 2021, doi: 10.1002/ADHM.202100302.

[121] S. Muro *et al.*, “Control of Endothelial Targeting and Intracellular Delivery of Therapeutic Enzymes by Modulating the Size and Shape of ICAM-1-targeted Carriers,” *Molecular Therapy*, vol. 16, no. 8, pp. 1450–1458, Aug. 2008, doi: 10.1038/MT.2008.127.

[122] S. Azarmi, W. H. Roa, and R. Löbenberg, “Targeted delivery of nanoparticles for the treatment of lung diseases,” *Advanced Drug Delivery Reviews*, vol. 60, no. 8, pp. 863–875, May 2008, doi: 10.1016/J.ADDR.2007.11.006.

[123] M. G. Toscano, D. Ganea, and M. Gamero, “Cecal ligation puncture procedure,” *J Vis Exp*, no. 51, 2011, doi: 10.3791/2860.

[124] S. et al Bilekova, “Pharmacological Targeting of Endoplasmic Reticulum Stress in Pancreatic Beta Cells,” *Trends in Pharmacaological Sciences*, vol. 42, no. 2, pp. 85–95, 2020.

[125] “National Diabetes Statistics Report Diabetes CDC.” https://www.cdc.gov/diabetes/data/statistics-report/index.html (accessed Jun. 29, 2022).

[126] A. Jurjus *et al.*, “Inflammatory bowel disease, colorectal cancer and type 2 diabetes mellitus: The links,” *BBA Clinical*, vol. 5, no. 2016, pp. 16–24, 2016, doi: 10.1016/j.bbacli.2015.11.002.

[127] G. Solinas and B. Becattini, “JNK at the crossroad of obesity, insulin resistance, and cell stress response,” *Molecular Metabolism*, vol. 6, no. 2, pp. 174–184, 2017, doi: 10.1016/j.molmet.2016.12.001.

[128] C. Ning *et al.*, “Chicory inulin ameliorates type 2 diabetes mellitus and suppresses JNK and MAPK pathways in vivo and in vitro,” *Molecular Nutrition and Food Research*, vol. 61, no. 8. 2017. doi: 10.1002/mnfr.201600673.

[129] S. E. Alavi and H. Ebrahimi Shahmabadi, “GLP-1 peptide analogs for targeting pancreatic beta cells,” *Drug Discovery Today*, vol. 26, no. 8, pp. 1936–1943, 2021, doi: 10.1016/j.drudis.2021.03.032.

[130] T. Bouckenooghe, D. Flamez, F. Ortis, S. Goldman, and D. L. Eizirik, “Identification of new pancreatic beta cell targets for in vivo imaging by a systems biology approach,” *Curr Pharm Des*, vol. 16, no. 14, pp. 1609–1618, Apr. 2010, doi: 10.2174/138161210791164117.

[131] L. Marselli, A. Piron, M. Suleiman, D. L. Eizirik, M. Cnop, and P. Marchetti, “Persistent or Transient Human Beta Cell Dysfunction Induced by Metabolic Stress: Specific Signatures and Shared Gene Expression with Type 2 Diabetes,” 2020, doi: 10.1016/j.celrep.2020.108466.

[132] F. K. Ndiaye *et al.*, “Expression and functional assessment of candidate type 2 diabetes susceptibility genes identify four new genes contributing to human insulin secretion,” *Molecular Metabolism*, vol. 6, no. 6, p. 459, Jun. 2017, doi: 10.1016/J.MOLMET.2017.03.011.